AFRICA CENTER OF EXCELLENCE FOR WATER MANAGEMENT
ADDIS ABABA UNIVERSITY

Performance and optimization study of Shaped Aluminum Hydroxide/Hydroxyapatite adsorbents for removal of Fluoride from Drinking Water

Shina Chepkemoi

Advisor; Dr Beteley Tekola (PhD)

A Master's thesis submitted to the Africa Center of Excellence for Water Management, Addis Ababa University in partial fulfillment of the requirements for The Degree of Master of Science in Water Management (Water Quality)

July 2024
Addis Ababa, Ethiopia

Africa Center of Excellence for Water Management

Addis Ababa University

Performance and optimization study of Shaped Aluminum Hydroxide/Hydroxyapatite adsorbents for removal of Fluoride from Drinking Water

By: Shina Chepkemoi

A Master's thesis submitted to the Africa Center of Excellence for Water Management, Addis Ababa University in partial fulfillment of the requirements for The Degree of Master of Science in Water Management (Water Quality)

Declaration

I, Shina Chepkemoi (GSR/1948/15), hereby declare that this MSc research titled ***"Performance and Optimization study of shaped aluminum hydroxide/hydroxyapatite adsorbent for removal of fluorides from drinking water"*** has been developed by me and has not been submitted to any other institution for award of any academic qualification. The content of this thesis has not been plagiarized and where works of other researchers have been used, they have been appropriately cited.

Candidate's Name_____ **Signature** _____ **Date** _____

AFRICA CENTER OF EXCELLENCE FOR WATER MANAGEMENT
ADDIS ABABA UNIVERSITY

Performance and optimization study of Shaped Aluminum Hydroxide/Hydroxyapatite adsorbents for removal of Fluoride from Drinking Water

By: Shina Chepkemoi

A MASTER'S THESIS SUBMITTED
TO
AFRICA CENTER OF EXCELLENCE FOR WATER MANAGEMENT
ADDIS ABABA UNIVERSITY

APPROVED BY BOARD OF EXAMINERS

This is to certify that we have read this MSc research and that in our opinion; it is fully adequate, in scope and quality, as a Master's thesis for The Degree of Master of Science in Water Management (Water Quality)

Advisor
Name _____Signature_____ Date_____

Co-Advisor
Name _____Signature_____ Date_____

Examiner
Name Dr. Anuradha Jabasingh Signature _____ Date 30th July 2024

Examiner
Name _____Signature_____ Date_____

Chairperson
Name _____Signature_____ Date_____

Acknowledgment

First of all, I am very grateful to Almighty God for gracing me with good health, guidance and wisdom throughout this research undertaking. Secondly, I would like to express my deepest gratitude to my advisor Dr Beteley Tekola (PhD) for his invaluable guidance, unwavering support, and constructive feedback throughout the course of this research. Thirdly, I am incredibly appreciative of the government of Ethiopia in collaboration with the World Bank Organization for providing the support needed to accomplish my master's degree.

I would also like to express my sincere gratitude to the Africa Center of Excellence for Water Management (ACEWM) for providing me opportunity to pursue my master's degree and moreover with resources and a helpful environment while conducting this research. The facilities and support offered by the center played a crucial role in the progression and completion of this master's thesis.

I am profoundly grateful to Professor Yonas Chebude, Hyredine Ismael, and the laboratory assistant Ms Elelta Aklilu, whose commitment and technical support were essential to the laboratory work's successful completion. I am also appreciative of the Addis Ababa Institute of Technology, specifically the Department of Biochemical Engineering, for letting me use their laboratory for a portion of my laboratory work. I am especially appreciative of Mr. Hintsasilassie for his assistance and commitment to ensuring that everything in the lab went as planned.

Lastly, I would like to thank my family and friends for their unwavering support and encouragement their belief in me provided the strength I needed to complete this research.

Table of Contents

List of Tables

List of Figures

List of Acronyms

$AlOH_3$/HAP – Aluminum Hydroxide /Hydroxyapatite

APHA –American Public Health Association

BDST –Bed depth service time model

CCD – Central Composite Design

EDTA- Ethylene diamine tetra acetic acid

FTIR – Fourier transform infrared

K – Kelvin temperature

K_α –BDST kinetic constant

K_{AB} -Adams –Bohart Kinetic constant

K_{TH} –Thomas Model Kinetic constant

K_{YN} –Yoon Nelson model kinetic constant

Mg/g –Milligrams per gram

Mg/L – Milligrams per liter

MTZ- Mass transfer zone

OSHO-Oromo Self-Help Organization

PH_{PZC} –pH point of zero charge

SEM – Scanning electron Microscopy

WHO – World Health Organization

XRD – X-ray diffraction

ABSTRACT

The study aimed to investigate the efficacy of shaped Aluminium Hydroxide/Hydroxyapatite composite adsorbent in fluoride removal in continuous column experiments. Spherical and cylindrical shapes of the composite adsorbent were produced and characterized for functional groups, phase composition, and structural characteristics. The performance of breakthrough curves was examined in a continuous column adsorption experimental setup by examining the effects of changing process factors such as flow rate, bed height, initial fluoride concentration, type of binder, and pellet shape. The analysis of the breakthrough curve revealed that the cylindrical pellets outperformed the spherical pellets in terms of adsorption capacities, with 1.34 mg/g and 0.679, respectively. Additionally, the results of the bentonite-binder pellets were significantly lower than those of the corn starch binder pellets. The adsorption capacity decreased with a rise in flow rate and initial fluoride contents and increased with rise in the height of bed. Adams-Bohart Model, Thomas model, and Yoon-Nelson model were used to model the breakthrough curve of different process parameters. The R^2 for the Adams-Bohart model was between 0.89-0.96 for different process conditions. The Yoon-Nelson and Thomas model yielded R^2 values ranging from 0.92-0.99 for all process parameters. The bed depth service time (BDST) model was employed to illustrate the impacts of bed height on the breakthrough curve and to forecast the breakthrough and exhaustion time of the adsorbent. The reliability of the model was demonstrated by a high R^2 value of 0.987. Central Composite statistical experimental design for optimization showed a good fit to the quadratic model with R^2 =0.97 and 1.41 mg/g adsorption capacity at optimum conditions of 15 ml/min flow rate, 10 cm bed height, and 5 mg/l fluoride concentration. Fluoride-saturated Al(OH)3/HAP pellets were successfully desorbed in three adsorption-desorption cycles using 10% sodium hydroxide; the desorption efficiency was 88% in the first cycle, 71% in the second, and 61% in the third.

KEYWORDS; $Al(OH)_3$/HAP adsorbents, binders, fluoride removal, Hydroxyapatite, Shaped adsorbents,

1.0 INTRODUCTION

1.1 Background

Groundwater and other geological settings contain naturally occurring fluoride (F^-). It aids in promoting the calcification of hard tissue and inhibits dental cavities, making it a necessary nutrient for humans when consumed within the suggested range. Conversely, however, too much fluoride in consumption can cause tooth and bone fluorosis as well as other health problems. Over two hundred million people globally are reportedly drinking water that contains higher levels of fluoride than the 1.5 mg/L WHO recommendation (WHO, 2004). This prompts questions regarding the necessity of efficient and long-lasting methods to ensure that fluoride consumption is balanced, maintaining its advantages while avoiding its negative consequences. Adsorption is the most appealing technology among the various defluoridation techniques due to its adaptability, low operating costs, ease of use, and sustainable fluoride removal. The process works by establishing chemical or physical bonds between a mix of liquid and a porous solid medium (Pang et al., 2021).

Fluoride removal from drinking water has been studied using a variety of adsorbents. These comprise hydrous zirconium oxide/polyacrylonitrile nanofiber (X. Wang et al., 2019), zinc-magnesium-aluminum ternary oxide microspheres (Gao et al., 2020), hydroxyapatite microspheres (Gao et al., 2019), metal-organic framework (Zhu et al., 2018), and engineered biochar (Jiang et al., 2018). However, there are some disadvantages to these adsorbents as well, such as high costs for upkeep and operation, secondary environmental contamination from the creation of hazardous sludge, and challenging treatment procedures (Bhatnagar et al., 2011).

In rural Ethiopia, defluoridation technology is being deployed. Activated alumina and diatomaceous earth are locally accessible materials that have been the subject of extensive investigation in addition to the Nalgonda approach. However, each of these inexpensive techniques has shortcomings, such as excessive operating expenses and ineffective fluoride elimination (Mulugeta et al., 2014). The Nalgonda technology has several limitations, such as producing large volumes of sludge, requiring constant supervision and expert staff to manage day-to-day operations, and being unable to treat raw water with elevated levels of total dissolved solids and concentrations of fluoride higher than 10 milligrams per liters (Zewge, 2016).

The Oromo Self-Help Organization (OSHO), a regional non-governmental organization (NGO), has made an effort to deploy boner char technology in field investigations at homes and community levels (Osterwalder et al., 2014). Hydroxyapatite has a large specific surface area and fluoride removal capability but due to its many uses in the biomedicine area, it is quite pricey, especially when importing input materials. Furthermore, due to cultural and religious views, cow bone char may be objectionable in some areas, including some regions of Ethiopia. Therefore, more research is needed to develop a fluoride elimination medium that is readily available locally and has a high fluoride absorption capacity so that it can be utilized in households and small communities to lessen the negative effects of fluoride.

The use of composite materials creates a synergistic effect between the materials hence promoting high adsorption performance and stability throughout the adsorption process. Aluminum hydroxide is cost-effective for production on a large scale since aluminum sulfate, which is produced locally, can be used as a precursor in creating aluminum hydroxide. Due to the aluminum and fluoride ions' high attraction to one another, adsorbents based on aluminum have comparatively large adsorption capacity but they have limitations (Wan et al., 2021). Lower pH levels are where adsorbents based on aluminum exhibit their great adsorption capability; nevertheless, aluminum can be released into the purified water at lower pH, which could be detrimental to human well-being (Mondal & George, 2015). As a result, post-treatment of the water is required, increasing treatment costs.

Hydroxyapatite has a high specific surface area, a porous surface, and a high ion exchange capacity, chemically stable, and the hydroxyl group of hap can readily be replaced by anion hence it has a high capability to bind fluoride ions (Raghav et al., 2018). However, its cost makes it unpopular and in certain regions including Ethiopia, hydroxyapatite has limited acceptance due to religious restrictions (Gwala et al., 2011). Additionally, hydroxyapatite cannot be utilized to remove fluoride in column studies due to its low mechanical strength (George et al., 2020).

Therefore, the disadvantages of utilizing just one adsorbent can be avoided by utilizing composites, which combine the benefits of both. As such, using Aluminium hydroxide/HAP as a composite adsorbent has the potential to be a useful adsorbent.

These composites are produced as powders, which presents several processing challenges when utilized in industrial applications.

1.2 Problem Statement

The composite adsorbent of Aluminium hydroxide and HAP shows promise in eliminating fluorides from drinking water (Opoka et al., 2023). However, the production in powder form, makes it not suitable for industrial applications as it results in many technical issues, they cause drops of pressure, clogging and handling difficulties, and release of powder into the treated effluent. It is also extremely difficult to recover them and involves additional costly separation steps, making them difficult for real-world use (Laonapakul et al., 2022).

Powdered adsorbents can build up and cause obstructions in the column which can hinder the flow rate and even result in an increase in system pressure. When significant obstructions occur, the increased burden on the pump's parts can potentially result in damage to the pump. (Lou et al., 2022). The obstruction also reduces the flow rate, affecting treated water volume. Oromo Self Help Organization (OSHO), a local business that supplies and installs HAP in Ethiopia, claims that the bone char filter can only produce 15–25 Liters of drinkable water per day.

Powdered adsorbents also have small particles and tight spaces which produce resistance to the flow of the liquid as it passes through the bed which gets worse as the bed gets more saturated necessitating high pressure to keep the flow steady which induces high-pressure drops (Opoka et al., 2023).

Researchers also have faced difficulties with the flow within the bed of adsorption and the powder's outflow into the treated water (Jo et al., 2021). This frequently reduces the adsorption effectiveness and impairs the material's performance (Guaya et al., 2022). While coating techniques like impregnation can immobilize the particles and remedy this problem, these methods frequently lead to issues with strength and stability, such as the coating layer coming off (Alagumuthu & Rajan, 2010). Furthermore, minimal amounts of active substances may be present in the final structure.

To address these problems, extrusion can be used to produce large amounts of structured adsorbents while preserving the mechanical strength of the formed material. This is achieved by adjusting the binder quantity in a recipe to guarantee that no appreciable loss in adsorption characteristics of the adsorbent occurs (Pereira et al., 2022). The powders are usually aggregated into pellets or granules, where the binders provide structural integrity and enhance the mechanical strength of the composites. Common binders include organic ingredients such as starch, dextrin, natural clays, and carboxymethylcellulose; synthetic materials such as silica, alumina, and polyalcohols like polyvinyl alcohol and its derivatives; and inorganic aluminosilicate clays such as bentonite, kaolin, and attapulgite (Fungaro & Bertolini, 2022).

Natural clays such as kaolinite and bentonite are frequently utilized as binders in shaping powders because they are not toxic and can also effectively adsorb pollutants. In addition, these clays are readily available, have a high specific area, are stable, and possess distinctive structural properties (Mustapha et al., 2019). Among the binders, many considerations go into the selection of bentonite and corn starch as binders because they are reasonably priced, conveniently accessible, and produced in an eco-friendly manner. Finally, they are both readily regenerable, and, more importantly, they can function as binders and adsorbents at the same time because they are utilized as adsorbents on their own (Uddin, 2017).

To date, several studies have utilized the composite of HAP and other materials; however, as far as this study is concerned, no studies have been conducted in the literature on the synthesis of shaped adsorbent of Aluminium hydroxide/hydroxyapatite composite via extrusion for defluoridation in column studies for fluoride removal.

Therefore, this study proposed the shaping of Aluminum hydroxide/HAP composite adsorbent powders via extrusion with natural bentonite and corn starch as binders, which can be scaled up for potential field applications and consequently address the challenges of powder adsorbent in column studies.

1.3 Research Questions

- How can a shaped aluminum hydroxide/hydroxyapatite composite (cylindrical and spherical shapes) adsorbent be prepared using corn starch and bentonite as binders at varying adsorbent-to-binder ratios?
- What are the mineralogical and morphological composition and structural characteristics of shaped $Al(OH)_3$/HAP composite adsorbent?
- How effective are the shaped Aluminum hydroxide/hydroxyapatite composite for the removal of Fluoride from water?
- What are the effects of different operation conditions on fluoride removal and optimal value for column adsorption?
- What are the isotherm kinetic and mechanism behaviors of fluoride adsorption on the shaped composites?
- How can spent $Al(OH)_3$/HAP adsorbent composite be recycled without altering the adsorption integrity?

1.4 Research Objective

1.4.1 General Objective

The general objective of this study was to evaluate the performance of shaped $Al(OH)_3$/HAP adsorbent composite by utilizing natural clay (bentonite) and corn starch for fluoride removal from drinking water in a continuous column experiment.

1.4.2 Specific Objectives

- To synthesize and characterize shaped (cylindrical and sphere) Aluminium hydroxide/Hydroxyapatite composite adsorbent using corn starch and bentonite as binders at varying adsorbent-to-binder ratios.
- To investigate the effect of the type of shape, type of binder, and adsorption operating conditions (flow rates, initial fluoride concentration, and bed height) on fluoride removal efficiency in a continuous system and determine optimal conditions using a central composite design
- To evaluate the isotherm kinetics and mechanism behavior of fluoride adsorption on the shaped $Al(OH)_3$/HAP adsorbent.
- To investigate the reusability of spent adsorbent in adsorption-desorption studies

1.5 Significance of the Research

The findings of this research will provide valuable insights for the design and fabrication of advanced adsorbents for practical use, knowledge creation, benefit to the community, attraction of interest to future investment, and decision-making towards adoption of efficient, low-cost, and sustainable water treatment technology for removing fluoride from drinking water.

1.6 Scope of the Study

This research study only focuses on the fabrication of shaped Aluminium Hydroxide/Hydroxyapatite composite adsorbent for the removal of fluorides from drinking water in continuous column adsorption experiment and the characterization of the shaped $Al(OH)_3$/HAP composite adsorbent. In addition, the study addresses the regeneration of spent adsorbent in adsorption-desorption studies, the examination of column data to investigate column performance, the development of adsorption models from the column data, the examination of process parameters in continuous column experiments, and the application of response surface methodology, central composite statistical experimental design to optimize these process parameters.

2.0 LITERATURE REVIEW

2.1 Fluoride-Related Issues

Fluorine is the thirteenth most widely found element. It is corrosive, chemically active, and exhibits strong chemical affinity. Trace amounts of this essential microelement are necessary for many organs in the body, especially the teeth and bones, to grow and develop regularly. On the other hand, prolonged exposure to high levels is bad for health. Among the exposure sources are food, water, air, and excessive toothpaste use. Although drinking water is the most popular method, other ways to take fluoride include toothpaste, tea, nicotine, milk, food, meat, and excessive beverage consumption (Mohammadi et al., 2017). The maximum permissible level of fluoride in drinking water, as determined by the World Health Organization, is 1.5 mg/L, (WHO, 2002). The subject of this issue is global in scope, the limit is exceeded in numerous locations across the world, such as the West Indies, China, Argentina, the Netherlands, Poland, India, Mongolia, Mexico, Italy, Spain, the United Kingdom, and several regions of Africa and America (Ali et al., 2016). Overexposure to fluoride can have negative implications on the nervous system, the endocrine system, and skeletal and dental fluorosis (Chavali et al., 2015).

According to the World Health Organization, drinking water should have a fluoride content of between 0.5 and 1.5 mg/L at a temperature range of 285 and 298K to sustain general health (WHO, 2011).

Table 1:Effects of fluoride concentrations in drinking water on human health

(Arya et al., 2021; Siaurusevičiūtė & Albrektienė, 2021; Singh et al., 2016 ;Jamwal & Slathia, 2022)

Level of fluoride (milligrams per gram)	Impacts on health
< 0.5	Inhibit the occurrence of tooth cavities
0.5 – 1.5	helps promote bone and dental health by promoting tooth and bone growth.
1.5 -4.0	Fluorosis of the teeth, particularly in children
4.0 - 10	Fluorosis in the skeleton and teeth
> 10	crippling fluorosis of the skeleton

2.2 Defluoridation Techniques

The main methods for defluoridation are reverse osmosis, ion exchange, adsorption, precipitation/coagulation, and electrodialysis.

2.2.1 Precipitation/Coagulation

The process entails combining lime, bleaching powder, and salts of alum with the standard water treatment. The process is based on removing the fluoride from the flocs after they are removed. Coagulation is the most affordable approach in low-income countries where the primary expenses of RO are prohibitive and society cannot afford to obtain and use RO for drinking water (Dubey et al., 2018) .The precipitation method's high chemical costs, batch process, creation of sludge with a high concentration of hazardous aluminum fluoride composite, inability to treat large volumes of water, unfavorable treated water taste, and high residual aluminum dose make it rarely employed. . (Yadav et al., 2018).

2.2.1.1 Nalgonda Techniques

The Nalgonda approach is employed in Senegal, Kenya, Tanzania, and India, among other nations, and is one of the most widely used precipitation/coagulation systems for defluoridation. The exact amounts of lime, alum, and bleaching powder to add to water are measured using this approach. The water is then treated using a combination of flocculation, sedimentation, filtration, and disinfection techniques (Tomar & Kumar, 2013).

2.2.2 Adsorption Method

This approach is very promising for getting rid of fluoride because of its potent removal powers, simplicity of application, low cost, and adsorbent renewal (Yadav et al., 2018).In literature, a variety of adsorbent materials has been used such as activated fly ash, carbon alumina, sawdust, and coconut shell carbon. Two of the most commonly utilized adsorbents are activated alumina and carbon (Razbe, 2013).

2.2.3 Ion exchange

The high cost of the resins makes this treatment procedure unfeasible, although they are readily regenerable. One drawback of this approach is the significant volume of sludge with a high fluoride content that is created during renewal and needs to be disposed of. However, the process's efficacy is fairly low and is significantly impacted by the existence of additional anions, including phosphates, nitrates, carbonates, sulfates, etc.) (Grzegorzek et al., 2020; Yadav et al., 2018).

2.2.4 Reverse Osmosis (RO)

It is a physical process that forces water through a semi-permeable barrier under pressure. of a particular size to remove dissolved sediments and other unwanted pollutants so that it can be

used in homes and businesses. Moreover, fluoride removal from drinking and industrial water has been accomplished with RO. The type of reverse osmosis membrane used depends on the kind of water to be purified, financial factors, and operational variables including pressure, temperature, and membrane recovery (Wimalawansa, 2013).

2.2.5 Electro dialysis

Dialysis uses a membrane to hold the solutes in situ based on how well they diffuse through it. The process is electrochemical which uses DC voltage to separate ions using resin membranes (Dhillon et al., 2017). Based on the charge of the ions that pass across them, two types of membranes are used in electrodialysis: cation and anion exchange membranes. Cations cannot flow through anion exchange membranes, and anions cannot pass through cation exchange membranes. Anions move to the anode and can cross anion exchange membranes with a steady electric field. Dilute and concentrate streams are created as a result. (Grzegorzek & Majewska-Nowak, 2016).

The adsorption process is among the most efficient physical processes because of its simplicity, technical viability, and operational flexibility. Local processing can produce inexpensive adsorbents from natural resources, industrial and agricultural wastes, and other easily accessible materials. These substances can be used to create shaped adsorbents, like the aluminum hydroxide/hydroxyapatite composite adsorbent, which has the potential to regenerate and has multiple advantages, such as a higher surface area and a greater affinity for fluoride ions, making it an economical and effective way to treat water.

2.3 Techniques for Synthesis of Shaped Adsorbents.

Powder shaping techniques with binders and without binders include granulation, Pelletization, extrusion, and spray drying.

2.3.1 Pelletization

It is a straightforward procedure that creates agglomerates by compacting powder particles via a die under pressure. It is also known as tableting, compressing, or pressing. Palletisation's primary goal is to create pellets that are closely packed for use in larger fixed-bed reactors. It is not necessary to use a binder for this technique, even if the compaction itself offers reinforcement. However, there are instances in which it is very beneficial to use binders to increase the mechanical stability of pellets. It operates using the same idea as granulation. The resultant agglomerates of the two processes differ in shape: granules are spherical, whereas pellets are cylindrical in most cases (Valizadeh et al., 2018).

2.3.2 Granulation

It is a method for increasing the size of powder materials into bigger agglomerates with a 2–20 mm size range. Wet granulation and dry granulation are the two forms of granulation. In wet granulation, the parent powder is first combined with water. The three basic stages of wet granulation are nucleation and wetting, consolidation and coalescence, and attrition and breakage (Valizadeh et al., 2018). Dry granulation, on the other hand, involves compressing a parent powder under high pressure, especially if the powder is incompatible with a solvent. Granulation is a commonly employed structuring process that yields beads that are spherical with a diameter of a few millimeters. Granulation can only occur with solvents and binders, which are also required for coagulation (Yeskendir et al., 2021).

2.3.3 Extrusion

In the extrusion process, parent powder and water are combined to create a paste, which is then run through a die. Extrusion is superior to granulation or Pelletization it can produce a body in a range of shapes, including cylinders, sheets, strips, and hollow tubes. Extrudates is the term for the shaped body (Ashouri et al., 2022; Lakiss et al., 2020). Manual extrusion involves using laboratory or home-made equipment. There are two categories of extruders: screw and piston.

2.3.4 Spray Drying

In this shaping process, a slurry is heated to atomize tiny droplets. The scattered powder is rapidly evaporating off the droplets, leaving behind dried powder. Food and pharmaceutical companies employ this technique (Sosnik & Seremeta, 2015; Vertruyen et al., 2018).

Table 2:shaping techniques, merits, demerits and dimensions of formed bodies

(Yeskendir et al., 2021, Ashouri et al., 2022; Lakiss et al., 2020)

Technique	Advantages	disadvantages	Shapes formed	Dimension (µm)
Pelletizing	It's an easy process that produces homogeneity in pellets that are created, and it works with or without binders.	Because of the pricey equipment and high-pressure application, it is not suitable for all materials.	Pellets	D=1500-3000 H = 1500-3000
Extrusion	Good spheres with a wide variety of final morphologies can be created with a fair degree of control over their size and shape.	Die swell results in an unequal distribution of sizes; sifting is required, and binders are typically needed.	Extrudates	D= 1000-50000 H=3000-30000
Granulation	Reactive extrusion is one alternative, and there are several shape options. It's also a continuous activity.	The process is only possible with the inclusion of binders and solvents; paste rheology is difficult to control.	Beads or granules	D=1000-20000
Spray drying	One-step synthesis, form, and continuous process are all possible without binders.	High energy costs and a product's sensitivity to operating feed rate, flow rate, and inlet temperature	Microspheres	D=20 -200

2.4 Challenges of using Powdered Adsorbents

A greater range of materials contain suitable active sites that can operate as binding sites, which makes powdered adsorbents more commonly utilized. In addition, they are porous and have a big surface area. (Dlamini et al., 2020). Particle parameters such as size, shape, and density present many obstacles to the practical scaling up of powder adsorbent.

Powdered adsorbents are without chemical and thermal stability when used alone. The rise in operating costs is contributed by their significant energy requirement to run the system, pumps, and power included. The huge quantities of adsorbents needed, make it quite costly as well. Other expenses that need to be included in the maintenance budget are cleaning, equipment replacement, and inspections (Azha et al., 2021) . Other difficulties with powders include hydrodynamic pressure loss and column blockage, which are brought on by the tiny size, irregular shape, or variable density of the powder adsorbent (Jawad et al., 2017).Furthermore, once powder adsorbents are depleted, they are difficult to replenish. Filtration has been used historically to separate powders, yet this method can cause blockage in the filters and even

powder loss hence they are usually discarded as sludge after being utilized in water treatment leading to secondary contamination. The difficulties involved in recovering spent powder and regeneration thereby restrict its applications in numerous sectors (G. Zhang et al., 2007). Moreover, powder adsorbents are not to be utilized directly in fixed beds due to their poor separation, reduced hydraulic conductivity , and inevitable leaching (Dou et al., 2011) In addition, a second procedure must be used to remove the powder from the treated water following the treatment, adding to the labour-intensive process of treating the water and extracting the particles. It can also be costly and time-consuming to filter or sediment the water to remove the depleted adsorbent (Jawad et al., 2017).

Processing barriers also such as dustiness, clogging, abrasion, mass loss, and handling and transit challenges make powder materials generally unsuitable for industrial usage (Valizadeh et al., 2018)

2.5 Types of Binders

Binder types are categorized as synthetic, inorganic, or organic. Among the organic binders are dextrin, carboxymethylcellulose, polyvinyl alcohols, starch, and chitosan. Aluminosilicate clays like bentonite, apulgite, and kaolinite, as well as synthetic compounds, are examples of inorganic binders (alumina, silica). The most often used inorganic binders are bentonite and kaolin, whereas the most frequently used organic binders are starch, polyvinyl alcohol, and chitosan. These materials can be coupled with other materials, employed only as binders, or a combination of these components (Fungaro & Bertolini, 2022).

Polyalcohols, like polyvinyl alcohol and its derivatives, like polyvinyl butyral, are good binder materials, but they are costly and not practical for use in industrial settings. They also have some disadvantages, like being highly soluble in water, which can cause the binding to break down when contact with water is inevitable (B. Zhao et al., 2012). Therefore, to get over these problems and all of their downsides, researchers frequently look at ways to alter and mix them with other binders.

For instance (Chanut et al., 2016) employed a three weight percent polymer blend containing a mixture of polyvinyl alcohol and polyvinyl butyral as a binder to agglomerate metal-organic framework; the findings showed structural degradation and a three percent reduction in particular regions and volume of micropore, which matched the binder amount. Also (Anbia & Aghaei, 2019) utilized various ratios of polyvinyl alcohol and polyethylene glycol to shape 13X zeolites for carbon dioxide adsorption. The features of the granules physically were assessed, and the findings indicated that while enhancing the content of the binder up to a point

improved the physical characteristics, going beyond that point resulted in a decrease in surface area, a reduction in mechanical strength after burnout, and a reduction in capability for carbon dioxide adsorption. After cellulose, chitin is the second most prevalent naturally occurring polymer, can be converted to chitosan via alkaline deacetylation (Pathan & Bose, 2018). Its inherent beneficial qualities for the creation of materials include biocompatibility, biodegradability, low cost due to natural availability, and high reactivity from the presence of several reactive functional groups (Dragan & Dinu, 2020). Apart from these advantageous characteristics, chitosan is derived from chitin, which is mainly obtained from crustacean shells. The extraction and purification process for chitosan can be expensive, and it is sensitive to pH. It also has limited mechanical strength because it disintegrates in high temperatures and moisture. Moreover, a chitosan-based binder makes it difficult to regenerate adsorbent because it impedes the desorption process. In a study by (Hong et al., 2013) Lithium manganese oxides were granulated with chitosan and cross-linked using 0.2 moles per liter of sulphuric acid, increasing the stability and surface area of the granules. Lithium manganese oxides were utilized as a binding material for lithium ions' extraction from saltwater. The granulated substance's adsorption capability matched that of the parent powder material.

2.5.1 Bentonite as Binder

Bentonite has been employed as a binder successfully in literature by many studies. For instance, in a study by (Bertolini et al., 2022) fly ash was used to synthesize zeolite-NaA, which was then formed into spherical granules with bentonite binder levels ranging from 5 to 10 percent weights. Pellets containing 10 percent bentonite performed the best in terms of water resistance and enough mechanical strength. In another study by (Jo et al., 2021) Sludge alum from a water treatment plant was pelletized utilizing the extrusion process and a bentonite binder. Bentonite was added in just the right amount to keep the pellets in their original shape and to increase their strength. The investigation found out that despite pellets reduced adsorption capacity and rate in comparison to powder adsorbents, their adsorption capacity for arsenic was found to be comparable to that of the commercial adsorbent.

2.5.2 Starch as a Binder

Naturally occurring starch is a polysaccharide molecule that comes from plants and it's inexpensive, renewable, biodegradable, and widely available. It contains about 70 to 80 percent of amylopectin and 20 to 30 percent amylose. Physical and/or chemical modification of starch is required to make it more soluble because it is hydrophobic (H. Zhao et al., 2022). Physical

modification of starches such as gelatinization, hydrothermal, and non-thermal procedure are easy and affordable because they do not require chemicals or even biological agents (Ashogbon & Akintayo, 2014).

The process of starch gelatinization entails the breakdown of intermolecular bonds in the presence of heat and water. This mechanism enables hydrogen binding sites to interact with more water. Heat causes the starch granules to swell and become hydrated, turning into a paste. (S. Wang et al., 2015). This procedure lengthens the starch particle's surface area, increasing its porosity, and roughness, and reducing its crystallinity, all of which increase the binding capacity.

The adsorption capacity of starch-based adsorbents is not the only important feature to consider while recycling them. Another important factor is how well they can be desorbed. Gunawardene et al. (2021) report that modified starch exhibits a desorption efficiency of 97 percent. By washing them with a reagent, these adsorbents can be recycled, making them renewable resources. Reagents like hydrochloric acid and sodium hydroxide (Dang et al., 2022), acetone (Mittal et al., 2018) can be used to accomplish desorption. Many researchers have applied starch from different plant sources, the most prominent is corn starch and it showed good performance for instance (Cho et al., 2020) utilized gelatinized corn starch to create a starch gel, which was then used to granulate hydrothermally-produced poly aluminum chloride. The granular and powdered forms of adsorbent were compared, and the results of the adsorption kinetics and adsorption isotherm showed that the powder form had faster fluoride adsorption kinetics, but the pellets had good adsorption capacity. Also (Z. Wang et al., 2020) evaluated the effectiveness of four organic binders, protein, starch, lignin, and molasses in pelletizing hydro char biofuels. Upon investigating the characteristics of the binder-based pellets, the study's findings showed that, in comparison to other organic binders, pellets using 20 percent starch as a binder had the highest equilibrium moisture level and superior mechanical strength. In a study (Pandharipande & Borkar, 2016) corn starch gel was added to the synthesized corncob composite adsorbent to pelletize the composites. The results demonstrated that the adsorbent, when synthesized in pellet form, had a large surface area, 17 percent more than the powder used in its synthesis and that the pellets retained their strength in aqueous solution. Additionally, the maximum uptake capacity was of corn starch, as starch is a very good adsorbent in and of itself.

2.6 Adsorption Kinetics Modelling for Column Adsorption

2.6.1 Breakthrough Curves

Models are usually used to forecast the breakthrough curves and explain adsorption dynamics. Breakthrough curves represent the relative effluent to fluoride content of influent (Ct/Co) as a function of time. It is influenced by experimental parameters including bed height, flow rate and ion concentration (Chen et al., 2015).

2.6.2. Bohart-Adams Model

Adams–Bohart's model expresses a linear relation between C_t/C_o and time. The model implies that the adsorption rate is directly proportional to the concentration of the adsorbing species and the residual capacity of the adsorbent (Bohart & Adams, 1920). The linear form of the Bohart-Adams model is expressed using equation (1).

$$\ln \frac{C_t}{C_0} = K_{AB} C_0 \, t - K_{AB} \, N_0 \frac{Z}{F} \qquad (1)$$

Z is the height of the bed, N_0 is the saturation unit (mg/L), F is the linear rate (cm/min), and k_{AB} model kinetic constant (L/mg min), Co is the inflow fluoride ions concentration in mg per liter.

2.6.3 Thomas Model

The Thomas model was used to determine the outflow's breakthrough curve for column adsorption operations. (Thomas, 1944). It is predicated on the idea that there is no axial dispersion and that the process adheres to Langmuir kinetics of adsorption-desorption. . Equation (2) represents the model's linearized form.

$$\ln\left(\frac{C_0}{C_t} - 1\right) = \frac{K_{Th} \, q_0 \, \omega}{Q} - K_{Th} \, C_0 \, t \qquad (2)$$

Q_0 (mg/g) is the bed's adsorption capacity and k_{Th} (L/min mg) is its kinetic coefficient.

2.6.4 Yoon and Nelson Model

This model states that the rate at which the likelihood of the adsorbate molecule's adsorption decreases determines the possibility that an adsorbate would breakthrough on the adsorbent and the adsorbate adsorption (YOON & NELSON, 1984). The linear form of the model is expressed with equation (3).

$$\ln \frac{C_t}{C_0 - C_t} = K_{YN} t - \tau K_{YN,} \qquad (3)$$

where t is the breakthrough time in minutes, τ indicates the time required for fifty percent of the adsorbates to breakthrough (min), and k_{YN} is the rate constant (min^{-1}).

2.6.5 Bed Depth Service Time(BDST) model

The bed depth service (BDST) model is based on the notion that the surface response between the unused capacity of the adsorbent and the substance being adsorbed regulates the adsorption (Altufaily et al., 2019). It is used to calculate the amount of time the adsorbent may absorb the adsorbates before it exhausts, hence determining the speculative performance of column adsorption. The model was proposed by (Hutchins, 1973) and its linear form can be represented by Equation (4)

$$t = \frac{N_o H}{C_o U} - \frac{1}{K_\alpha C_o} \ln\left(\frac{C_o}{C_b} - 1\right) \qquad (4)$$

In this case, k_α is the BDST model rate constant (L/mg/min), No saturation concentration in mg/l, U is the linear velocity (cm/min), H is the bed height in cm, and C_o is the initial concentration and C_b is the breakthrough concentration.

The critical bed depth (Ho) was determined using Equation (5), which refers to the depth of the adsorbent bed in the column that is necessary to guarantee that the effluent concentration stays below the allowable value (1.5 mg/l) (Kumari et al., 2021).

$$H_o = \frac{U}{K_\alpha N_o} \ln\left(\frac{C_O}{C_b} - 1\right) \qquad (5)$$

2.7 Effects of Process Parameters on Breakthrough Curves.

2.7.1 PH of Ethiopian Rift Valley Groundwater Samples

Studies have shown that the PH of influent water can significantly impact the adsorption capacity of adsorbents in column experiments. Real groundwater samples from different locations often exhibit varying PH levels. In column experiments, adsorbents have shown divergent performance based on various PH of groundwater samples. For instance (Dessalegne et al., 2016) conducted a column experiment using calcined layered double hydroxide on groundwater from the Ethiopian Rift Valley that had a pH of 8.5 and 10.5 mg/l fluoride

concentration at room temperature. It was possible to remove fluoride up to 2.2 mg/g at its maximum.

(Kebede et al., 2016) investigated fluoride removal experimentally using groundwater samples from the Ethiopian Rift Valley town of Nazareth, with an initial fluoride concentration of 14.22 mg/L and a pH of 7.76. Iron ore was used as an adsorbent, and an 89 percent removal efficiency was found. In a different study conducted by Regassa et al. (2016), groundwater samples with an initial pH of 7.87–7.94 and a fluoride level of 15.3 mg/l were taken from Jimma. With natural coal adsorbent and activated coal adsorbent, respectively, the fluoride level was successfully lowered to 5.814 and 1.836 mg/l at room temperature. In a study by (Zewge ,2016) investigations were conducted into the effectiveness of hybrid aluminum sulfate/hydro(oxide) in eliminating fluoride from groundwater samples sourced from six community water supply schemes chosen within the Rift Valley Region. With starting fluoride concentrations ranging from 8.87 mg/L to 25.4 mg/L and water samples' PH ranging from 6.51 to 8.74, an 85–93 percent removal effectiveness was achieved.

2.7.2 Initial Ion Concentration

Exhaustion points and breakthrough points happen faster at higher initial influent concentrations, according to several studies. Because there are initially many sites available for adsorption, adsorption proceeds quickly; but, as concentration grows, sites exhaust more quickly, resulting in a decrease in the volume of effluent; so, breakpoint time also lowers as inlet concentration increases (Maleki et al., 2021).

2.7.3 Flow Rate

At a higher flow rate breakthrough occurs faster because as the flow rate increases, the mass transfer also increases which accelerates the saturation of the adsorbent (López-Cervantes et al., 2018). At low flow rates, adsorbate has more time to come in contact with the adsorbent which increases the removal of adsorbate in the column (Sheng et al., 2018).

2.7.4 Height of the Bed

Increasing the column's bed height delays the onset of breakthrough and exhaustion points since it provides more contact time between the sorbent and the pollutant being removed. It also increases the volume of water treated because of increased surface area and the number of binding sites available for adsorption and also because as the quantity of adsorbent increases the duration time for interaction also increases (Maleki et al., 2021).

2.8 Regeneration of Adsorbents

Regeneration is the term used to describe the expeditious recovery or recycling of used adsorbents using commercially and technically viable techniques. The technique of removing contaminants from aqueous solutions is straightforward, but desorption is still difficult because of the strong attraction that adsorbates have for the surface of the adsorbent.

Thermal regeneration, steam regeneration, pressure swing regeneration, vacuum regeneration, microwave regeneration, and ultrasonic regeneration are some of the regeneration techniques that are accessible.

In the process of regeneration, cost is an important consideration, and the simplest and most economical way is chemical regeneration. Bases, acids, or salts can all be used in this process. (Kanyora et al., 2014) .Since strong acids might cause the adsorbent to leach, the best way to regenerate spent adsorbent is to employ caustic soda which can replace hydroxyl ions with fluoride ions. Sodium hydroxide concentrations ranging from 10 % to 1.5 moles per liter are often utilized for regeneration because these lower concentrations minimize structural alteration of the adsorbent (Nur et al., 2014)

After a few cycles, the regenerated adsorbent's adsorption capability decreases because fluoride ions are not entirely removed by the eluent. The amount of times regenerated sorbent can be used is limited by the amount of hydroxyl ion accumulation on the adsorbent, which reduces its defluoridation capacity (Vivek Vardhan & Srimurali, 2016). Sorbents have been regenerated successfully by different research for instance in a study conducted by (Jin et al., 2014) synthesized modified kaolin clay used to remove chromium (VI) from an aqueous solution was desorbed by conducting experiments using sodium hydroxide, nitrate, chloride and carbonate with 10 % concentrations. The investigation showed that the chromium(VI) loaded adsorbent was successfully recovered with sodium carbonate with a maximum desorption efficiency of 86.53 percent. In another study by (Lin et al., 2018) Researchers employed different concentrations of sodium hydroxide as eluent for CeO2/SiO2 adsorbent and found that as the concentration of sodium hydroxide increased the desorption effectiveness also increased and with 10 percent sodium hydroxide using the experiment was conducted four times with almost no change in desorption efficiency of about 95 percent as the number of cycles progressed.

The reagents sodium hydroxide, hydrochloric acid, nitric acid, distilled water, methanol, and ethanol are frequently used to renew spent starch-based adsorbents. The desorption capacity of regenerate adsorbents has been assessed in numerous investigations throughout several cycles. (Zheng et al., 2023) used pure water and 50 percent sodium hydroxide to renew an adsorbent

based on starch. With very little adsorption capacity loss throughout five successive sorption-desorption cycles, the adsorbent performed admirably.

The fabrication of a shaped aluminum hydroxide/hydroxyapatite composite adsorbent for eliminating fluoride from drinking water and investigating how the shaping of the adsorbent influences their performance for fluoride removal in drinking water was the identified gap for this research endeavors after conducting the literature review. Therefore, to fill this gap, this research work fabricated a shaped composite adsorbent of Aluminum Hydroxide/Hydroxyapatite using bentonite and corn starch binders into spherical and cylindrical shapes and tested their efficacy in fluoride removal in continuous column adsorption. This method is both economical and environmentally friendly, and effective in fluoride removal and it overcame the challenges of using the powdered form of this adsorbent in column adsorption, as stated in the problem statement. Furthermore, the fabricated-shaped adsorbent can be easily scaled up for potential field applications.

This chapter has covered fluoride-related problems, different methods for synthesis of shaped adsorbents, problems with powdered adsorbents, types of binder for shaping adsorbents, Adsorption models, how process parameters affect breakthrough curves, and adsorbent regeneration. The chapter has also explained the various methods of removal of fluorides, the present study selected adsorption among the techniques reviewed because of its advantages, and the research gaps in the synthesis of shaped aluminum hydroxide/hydroxyapatite composite adsorbents from the literature were identified and addressed by this investigation.

In the subsequent chapter of this study, the emphasis was on the preparation of bentonite and corn starch binders, the synthesis of the Aluminium Hydroxide/Hydroxyapatite composite adsorbent, the shaping of the Aluminium Hydroxide/HAP composite adsorbent, the characterization of the shaped $Al(OH)_3$/HAP composite adsorbent, the experiment's statistical design for process parameter optimization, the column adsorption experiment to examine various process parameters, and, lastly, the regeneration of spent adsorbent in adsorption-desorption research.

3.0 EXPERIMENTAL

3.1 Reagents and Chemicals

Aluminum sulfate (97%) produced in the Awash Melkasa Aluminum Sulphate and Sulphuric Acid Factory was obtained from the Addis Ababa Water and Sewerage Authority and used in the synthesis of Aluminum hydroxide. The hydroxyapatite pellets produced by chemical precipitation were utilized exactly as received from the Oromo Self-Help Organization (OSHO) in Modjo, Ethiopia aside from crushing and sieving. The rest of the chemical used were purchased from the Ranchem industry and trading company in Addis Ababa city and they were all analytical reagents. It included sodium carbonate and bicarbonate (99.5%), caustic soda (98%), sodium fluoride (98.0%), trisodium citrate (99%), EDTA (99.4%), acetic acid (99.5%), and sodium chloride (99.8%). Commercial corn starch was also purchased from the local market.

3.2 Materials Preparation

3.2.1 Collection and Pre-treatment of Binders

Bentonite clay was collected from the Ethiopian Geological Survey. The clay was first crushed into powders and sieved through a sieve size of 600µm-150µm to obtain the homogeneous particle sizes. The starch gel was prepared through a gelatinization process, mixing 150g of starch powder with 150ml of deionized water and then the suspension was heated in a hot plate unistirrer at 85^{o}C while stirring it continuously for 20 minutes (Cho et al., 2020).

3.3 Synthesis of Aluminium Hydroxide/HAP Composite Adsorbent

Aluminium Hydroxide/HAP Composite Adsorbent was prepared following the protocol mentioned by (Opoka et.al 2023) Aluminium hydroxide was synthesized from Aluminium Sulfate via the precipitation method Appendix Fig 11. 0.1 kilograms of Aluminium Sulfate was dissolved in half liters of deionized water while being continuously stirred using a magnetic stirrer until it is dissolved completely. The resultant pH (2.7) was adjusted to pH 7, using 2M Sodium hydroxide. pH of 7, because Aluminium hydroxide stabilized at that pH (Mulugeta et al., 2014). NaOH solution was added dropwise using a burette to the base material to prevent flocculation. After a pH of 7 was attained, the solution was then left to age for half a day. The precipitate was then filtered, washed and rinsed with deionized water, and oven-dried at 373K for another half a day to form Aluminium Hydroxide. The solid formed was then crushed and sieved through a 600µm-150µm aperture sieve to obtain very fine particles. Hydroxyapatite was used without further treatment, it was crushed and sieved through the same sieve of

600µm-150µm and then mixed in a ratio of 30%$Al(OH)_3$/HAP. This ratio was adopted from (Opoka et al., 2023), where higher efficiency was recorded for fluoride removal.

3.4 Preparation of Shaped $Al(OH)_3$/HAP Adsorbent Composites

The 30%$Al_2(OH)_3$/HAP composite powder was mixed with each of the binders separately with varying binder percentages and preliminary experiments were conducted on the binder percentage in the composite to determine the optimal binder percentage.

The composite adsorbent was combined with deionized water in dry mass to a volume ratio of one-to-one. Various percentages of bentonite binder, 5 wt.%, 10 wt.%, and 15 wt.%, were thoroughly mixed with the adsorbent and the resulting semi-solid molds were then placed into locally made shaping equipment to create pellets, which were then immediately oven-cured at 100°C for two hours. Following that, the samples were removed from the oven and given time to cool before being put away in a plastic Ziploc bag so they could be used later.

To use corn starch as a binder, adsorbent composites were mixed with the starch gel that resulted from gelatinization until a homogenized mixture was created. The produced semi-solid mold was transferred also to locally made shaping equipment, and the formed pellets were promptly oven-dried for 12 hours at 60°C (Cho et al., 2020) and then stored in plastic ziploc bags ready for use. With both binders, the $Al(OH)_3$/HAP adsorbent composites were shaped in spherical and cylindrical shapes, shaping procedure shown in (Appendix figures 12 and 13) and then fluoride removal efficiency was investigated in a continuous column experiment.

The shaping equipment was fabricated by the technical assistant in the Department of Mechanical Engineering at Addis Ababa Institute of Technology. The shaping equipment for cylindrical shape was a flat aluminum plate which consisted of a total of 27 circular dies each 5 mm in diameter and 1cm deep for placing the adsorbent and pushing the material through the dies, Appendix Figure 13.

For spherical shape forming the equipment consisted of two aluminium plates each with 7 parallel grooves 5 mm in diameter. The bottom plate was slightly larger but had matching grooves with the top plate this allowed for manual use of the top plate to press the adsorbent down and controlled sliding along the grooves from the top towards the bottom to shape the material into spheres as shown in the appendix figure 12.

3.5 Characterisation of Shaped $Al(OH)_3$/HAP Composite Adsorbent

To evaluate the pellets' capacity to endure the force and retain their structural integrity throughout handling, the drop test (Fungaro & Bertolini, 2022; Gul et al., 2015) was employed to assess the stability of the pellets in water and the capacity of the pellets to retain their structural integrity following fluoride adsorption, the pellets were submerged in aqueous water containing 10 mg/l fluorides for one day (Laonapakul et al., 2022). In the drop test, ten pellets for each binder were randomly chosen from each batch, and then each pellet was dropped to the ground. Averaging the quantity of drips was done after a visual inspection of the breaking. Four drops are the standard quantity of drops for pellets (Gul et al., 2015).

To determine the impact of pH on pellet adsorption of fluoride, a point of zero charge was employed by salt addition method using 10% sodium chloride solution from pH 2–11. Pellets (0.2 g) were weighed and added to 50 ml of the 10 % NaCl solution. 10% NaOH and or HCl was then added to correct the pH. In each beaker, the initial pH was labeled as pH initial and was shaken for a day at room temperature at 200 revolutions per minute. Next, each bottle's pH was measured and marked as its final pH. The difference in pH was then computed, and a graphic was made to show the pH change versus the original pH (Laonapakul et al., 2022).

Fourier Transform-Infrared on PerkinElmer's Spectra 65 FT-IT, with a resolution of 4 $cm^{-1,}$ and four scans in KBr pellets, in the 4000-400 cm^{-1} range were employed to characterize bonding patterns and functional groups. The infrared was captured by scanning the adsorbent and the generated data was processed, peaks, bands, and spectral features were analyzed. The characterization was done in the faculty of chemical and physical science in the College of Natural and Computation Sciences. In the characterization procedure, after the pellets were crushed, they were combined with the KBr powder, formed into pellets using a pellet die and then put in a pellet holder for examination.

The X-ray Diffractometer Miniflex 600 was employed to assess the adsorbent's crystallinity. The copper X-ray tube generates the X-ray which is directed to the sample after being filtered by a monochrometer to increase the sensitivity; collimated to concentrate and its 2-theta position provides a distinct fingerprint of phases present. The intensity and peak spread were used to characterize the adsorbent (Soumen, 2022). The sample was crushed and grounded with a pestle and mortar to obtain fine powders for better diffraction patterns and then taken to the chemistry department on campus.

A scanning electron microscope (SEM) was utilized to investigate the adsorbent's surface morphological properties. The signal generated from the contact of the sample with a secondary electron detector provided two-dimensional images with information about the sample (Ariffin

et al., 2021). The SEM characterization was done at Adama Science and Technology University (ASTU).

3.6 Adsorption Experiment

3.6.1 Fluoride Stock Solution and TISAB Preparation

For analysis of fluorides, various concentration of the working solution was created by dilution method from the stock solution of fluoride, which was prepared by dissolving 220 milligrams of sodium fluoride in one liter of deionized water.

For tisab solution, 7g of trisodium citrate, 58g of sodium chloride, 2g of EDTA, and 57 ml of acetic acid were combined in a one-liter volumetric flask to create the total ionic strength adjustment buffer. 5 moles per liter of caustic soda was utilized to raise the resulting pH of 3.0 to a range of 5.3-5.5, and then the volumetric flask was filled to the appropriate level.

Fluoride standards with concentrations of 1 and 10 parts per million were used to calibrate the ion-selective electrode. A tisab buffer was added to 5 milliliters of the sample in a one-to-one ratio to prevent ionic interferences.

3.6.2 Continuous Column Experimental Set-up

For the column experiments, a column adsorption setup was used to carry out continuous column experiments at ambient temperature using a plastic column of 3.4 cm internal diameter and 18 cm in length. A schematic representation of the experimental configuration is shown in Figure (1) The bottom of the column was packed with cotton wool 1.5 cm high to prevent loss of adsorbent to the treated water, and a known mass of adsorbent was crammed into the column at different bed heights of 5 cm, 7.5 cm, and 10 cm. The top of the column was also filled with cotton wool to distribute equally the influent in the column. Deionized water was used to establish a state of balance in the column by pumping it through the column until the packed column was fully soaked with liquid.

A peristaltic pump with a controlled flow rate was used to pump fluoride working solution with concentrations of 5 mg/l, 10 mg/l, and 15 mg/l spiked carbonates and bicarbonates (10 mg/l) in an up-to-down manner at flow rates of 15 ml/min, 20 ml/min, and 25 ml/min. The concentration of fluoride was monitored by collecting effluent samples at the bottom of the column after every 15 minutes. The process was continued until the concentration level of fluorides in the effluent was almost equal to the influent amounts.

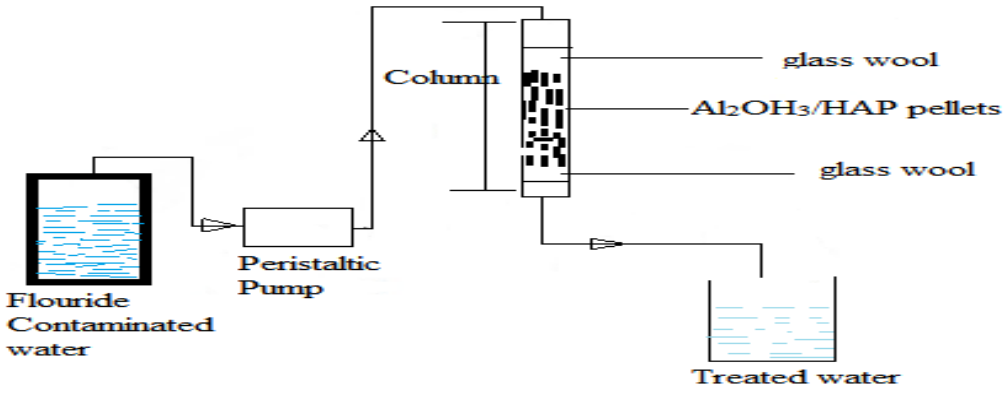

Figure 1: Schematic illustration of continuous column experimental setup for removal of fluorides with $Al(OH)_3$/HAP adsorbent pellets

The breakthrough concentration was characterized as 1.5 mg/l, the WHO recommendation as the maximum acceptable limit in drinking water (WHO, 2004). The breakthrough concentration (C_b) was considered as when C_t/C_o=0.15 while the exhaustion concentration (C_e) was characterized as when C_t/C_o =0.95. Whereby C_t represents the concentration of fluoride at any given time, t, and C_o is the inlet concentration. Plots of Ct relative to Co against time were used to create breakthrough curves.

After the adsorption experiment the effluent was analyzed and characterized for physical and chemical characteristics including pH, electrical conductivity, total dissolved solids, carbonates, bicarbonates, total alkalinity, and the presence of calcium, phosphates, and aluminum were analyzed according to the standards set forth by the American Public Health Association (APHA).

3.6.3 Column Data Analysis

For the determination of columns' adsorption capacity, an analysis of breakthrough curves parameter was done it includes; the exhaustion time (t_e) and treated volume at exhaustion time (v_s) were characterized as the time and volume at which the outlet fluoride concentration (C_t) reaches ninety-five percent of the initial concentration (Ct/Co = 0.95). Breakthrough time (t_b) and treated volume at breakthrough (v_b) were characterized in the study as the time and volume at which the effluent fluoride concentration (Ct) reaches fifteen percent of the initial fluoride concentration (Ct/Co = 0.15). The association between fixed-bed adsorption and breakthrough curve type was represented by the mass transfer zone (MTZ) (Patel, 2019).

The kinetic Models were employed by linear plots of the model according to equations (1), (2), and (3) respectively for various process parameters. The Adams-Bohart model was developed

by creating linear plots of ln(Ct/Co) against t at varying process factors and then from the intercept and slope, maximum adsorption capability (No) and the kinetic constant (K_{AB}) were obtained, the various factors of the Thomas model, the fluoride ion maximal solid phase concentration, rate constant (K_{TH}), Q_o (mg/g) was determined from intercept and slope of the linear plots of ln [(Co/Ct) -1] verses t and Yoon-Nelson model parameter K_{YN} values and ꚍ were calculated from the linear plots of ln [Ct/(Co-Ct)] versus t.

The linear plot of service time (t) versus bed depth (H) was used to calculate BDST model parameters, that is, saturation concentration (No), critical bed depth (Ho), and kinetic rate constant (k_α) according to equations (4) and (5) at breakthrough concentration (C_t/C_o=0.15) and exhaustion point (C_t/C_o=0.95).

In this study, breakthrough time was determined as the period when the effluent concentration (Ct) is equal to the breakthrough concentration (C_b) determined as 1.5 mg/l (WHO,2004). The adsorption capacity at the breakpoint and exhaustion point found out by calculating the area under the breakthrough curves using equations (6) and (7) respectively (Mehta et al., 2023; Mohan & Dutta, 2020; Mondal et al., 2018).

$$q_b = \int_0^{t_b} \frac{C_0 - C_t}{M}\, dt \qquad (6)$$

$$q_e = \int_0^{t_e} \frac{C_0 - C_t}{M}\, dt \qquad (7)$$

Q_e is the adsorption capacity at exhaustion time, and Q_b is the adsorption capacity at breakthrough time (t_b) in milligrams per gram (t_e). M is the mass, expressed in grams, of the adsorbent in the column.

Equations (8) and (9) were used to compute the amount of effluent treated at the point of exhaustion (Ve) and the breakthrough volume (Vb) that is the treated amount of effluent at the breakthrough point in liters when Ct/Co =0.15 treated (Golie & Upadhyayula, 2016)

$$\boldsymbol{V_e = Qt_e} \qquad (8)$$

$$V_b = Qt_b \quad (9)$$

To demonstrate the column's effectiveness, equation (10) below was used to compute the length of the mass transfer zone (Hernandez-Eudave et al., 2016).

$$MTZ = \frac{(t_e - t_b)}{t_e} * h \quad (10)$$

Where the breakthrough time is denoted by t_b, and the exhaustion time by t_e and the height of the bed in centimetres is donated by h.

The Empty bed Contact Time which is the duration of interaction between $Al(OH)_3$/HAP pellets and fluoride ions was determined using equation (11) (Geleta et al., 2021a).

$$EBCT = \frac{V_B}{Q} \quad (11)$$

Q is the influent rate of flow in milliliters per minute and V_B is the bed volume in millimeters and

3.7 Design of Experiment

The design of the experiment for investigating the effect of shape, binder–to–adsorbent ratio, and type of binder depending on a single variable at a time, keeping all other variables constant to narrow down the long list of potentially important factors to only a few important ones.

Except for the effects of binder ratio, the impact of every additional factor was tested in a continuous column adsorption experiment and after the most effective factor in terms of shape, binder ratios, and type of binders was identified, central composite statistical experimental design (CCD) under Response Surface Methodology (RSM) was utilized to optimize process parameters including bed height, flow rate, and starting fluoride concentrations to find optimal operational conditions for the column. The selection of CCD was based on its capacity to fit quadratic models, cut down on the quantity of trial runs needed to maximize effective factors, and investigate the interplay between parameters.

Runs of nc center, 2n axial, and 2n factorial are present in CCD. Factorial points represent the main combination of factors, (high and low levels), the center points estimate error and not well-fitted model and the data's repeatability, and the axial points are separated by a distance (α) from the center point along each factorial axis, the α values determine how far the axial point is from the design space's center (Mourabet et al., 2017).

The study modeled the concurrent impact of the independent variable which is fluoride initials concentration, flow rate, and bed height on the response variable which was the adsorption

capacity. The independent factors were implicit at five levels (-α, -1, 0, +1, +α) as shown in Table (3).

Table 3:Al(OH)$_3$/HAP composite adsorbent's implicit levels for independent factors

Factors	Levels				
	-α	**-1**	**0**	**+1**	**+α**
Flow Rate (A)	11.59	15	20	25	28.41
Bed Height (B)	3.30	5	7.50	10	11.70
Initial Fluoride Concentration (C)	1.59	5	10	15	18.41

Preliminary studies were used to determine the lowest and maximum values assigned to each factor. Twenty experiments in total, including 8 factorial points, 6 central points, and 6 axial points were chosen at random following the CCD described in Table (4).

Equation (12) below describes a second-order polynomial model that was made and experimental data was fitted to it.

$$\boldsymbol{\gamma = \beta_0 + \beta_1 A + \beta_2 B + \beta_3 C + \beta_{11} A^2 + \beta_{22} B^2 + \beta_{33} C^2 + \beta_{12} AB + \beta_{13} AC + \beta_{23} BC} \quad (12)$$

A, B, and C are the independent variables' implicit values, Y is the response variable expected, and the coefficient constant is denoted by β_0, the interaction coefficient is denoted by $\beta_{(12,\,13,\,23)}$, coefficients of the quadratic is denoted by $\beta_{(11,\,22,\,33)}$ while the linear coefficients are denoted by $\beta_{(1,\,2,\,3)}$ (Baharlouei et al., 2018; Sugashini & Sheriffa Begum, 2013; Xiao et al., 2013).

Analysis of variance(ANOVA) was used to validate the model and determine the statistical significance of the equation. Version 6.0.8 of the Stat-Ease, Design Expert software was used to analyze the experimental data.

Table 4:Fluoride adsorption onto $Al(OH)_3$/HAP composite adsorbent pellets Central Composite Design experimental design matrix

RUN	Factors			Response
	Flow Rate (A)	Bed Height (B)	Initial Fluoride Concentration (C)	Adsorption Capacity
1	11.59	7.5	10	
2	20	7.5	18.41	
3	15	5	15	
4	20	11.7	10	
5	15	10	15	
6	20	7.5	10	
7	25	5	5	
8	20	7.5	1.59	
9	25	5	15	
10	20	7.5	10	
11	20	7.5	10	
12	20	7.5	10	
13	28.41	7.5	10	
14	20	7.5	10	
15	20	7.5	10	
16	25	10	5	
17	15	5	5	
18	20	3.3	10	
19	25	10	15	
20	15	10	5	

3.8 Regeneration of Adsorbents

The fluoride-saturated column was desorbed in an up-down mode with an eluent of 10% caustic soda at a flow rate of 15 ml/min to ensure the least amount of eluent feasible used by the desorption process. The eluent solution was introduced into the column at room temperature at a 15 ml/min flow rate and the amount desorbed was monitored by collecting the sample from the column outlet at 15-minute intervals until a concentration of 0.15 the safe threshold that the World Health Organization recommends (WHO, 2004), was attained. The amount desorbed and desorption efficiency after each time were calculated using Equations (13) and (14) respectively (Baharlouei et al., 2018). After the elution process, the column was washed with deionized water at 15ml/min until the effluent's pH reached a neutral level (pH 7). These cycles were repeated for three cycles for the regeneration study.

$$Q_{desorbed} = \frac{Q}{1000}\int_{0}^{t=total} C_t\, dt \tag{13}$$

$$(\%)Desorption\ efficiency = \frac{Amount\ desorbed}{Amount\ adsorbed} * 100 \tag{14}$$

4 Results and Discussion

4.1 Characterization of $Al(OH)_3$/HAP Pellets

The $Al(OH)_3$/HAP composite adsorbent pellets were characterized by point of zero charge, FTIR, XRD, and SEM techniques to understand the surface charge, functional groups, crystalline property, and morphology of the shaped adsorbents.

4.1.1 Point of Zero Charge

The pHpzc values and Al(OH)3/HAP composite adsorbent pellets point of zero charge were examined to precisely comprehend how pH affects the adsorption of the adsorbent**.** As shown in Figure (2) the observed pHpzc value of $AlOH_3$/Hap pellets was 7.75. For the pellets in powder form, the point of zero charge was 7.4. (Opoka et al., 2023). This little rise after pellet formation may be the consequence of modifications to the composite material's surface following the addition of binder. The polysaccharide corn-starch, which has multiple hydroxyl groups, may have interacted with the surface hydroxyl groups of the composites, altering the surface charge by reducing the availability of acidic protons and raising the pHpzc value of the pellets relative to the powder form of the composite (Laonapakul et al., 2022) reported similar observations.

According to the point of zero charge tests, the surface of the $Al(OH)_3$/HAP composite adsorbent pellets becomes +vely charged whenever the solution's pH falls below 7.75, which increases the amount of fluoride ions adsorption through improved electrostatic interaction of the fluoride ions with the adsorbent (Geleta et al., 2021a) and above 7.75 the adsorbent surface will acquire a negative charge creating a repulsion with the fluoride ions (Elouahli et al., 2018)

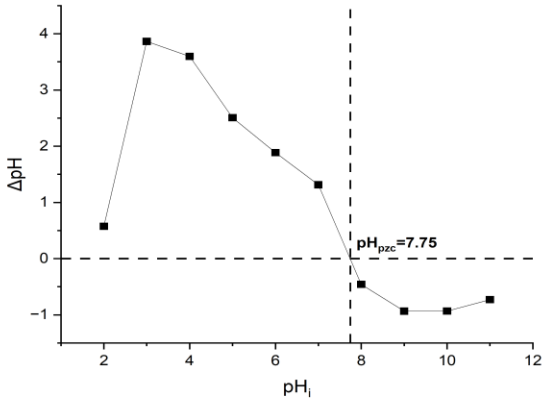

Figure 2: point of zero charge characterization for $Al(OH)_3$/HAP composite adsorbent pellets

4.1.2 FTIR Characterization

Figure (3) shows the spectra of FTIR of $Al(OH)_3$/HAP composite adsorbent pellets before adsorption, after adsorption, and after regeneration.

The hydroxyapatite's OH groups' vibrational and stretching modes are identifiable at the wide-ranging band seen at approximately 3412 cm^{-1} and 603 cm^{-1} (Coelho et al., 2019) . The phosphate group in apatite exhibits a symmetric stretching mode at approximately 1046 cm^{-1}, while the symmetric P-O stretching vibration of the group is observed around 565 cm-1 and 871 $^{-1}$ (Abifarin et al., 2019).

The bands at 1466 and 1424 are indicative of the presence of carbonate groups (Ahmed et al., 2015) which could have resulted from some hydroxyl ions from the solution reacting with ambient carbon dioxide, incorporating carbonate ions in the hydroxyl sites. The peaks observed around 1617 cm^{-1} and 1638 cm^{-1} are due to the stretching vibrations of water (Saikia et al., 2022). The asymmetric stretching vibrations of the C-H groups found in the glucose unit of corn-starch binder, a polysaccharide, are linked to the peaks at 2924 cm^{-1} and 2851 cm^{-1} (Baharlouei et al., 2018).

The position of peaks in the spectra obtained after adsorption decreased, which may have resulted from the creation of OH-F bonds and fluoride ions replacing hydroxyl ions in the adsorbent to create Fluorapatite ($Ca_5(PO_4)_3F$). Each of the peaks matched those found in the literature. (Mondal et al., 2018).

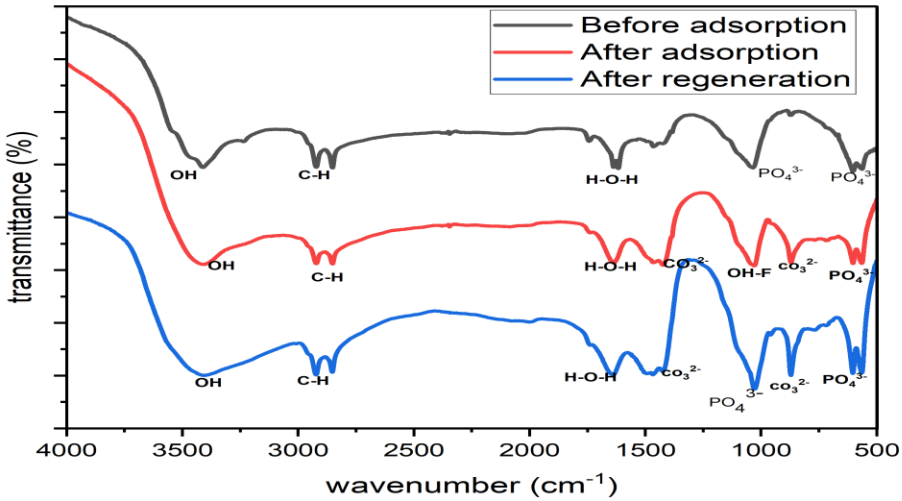

Figure 3: FTIR spectra for $Al(OH)_3$/HAP pellets for before adsorption, after adsorption and after regeneration

4.1.3 XRD Characterization

The XRD pattern for Al(OH)3/Hap pellets adsorbent before and after adsorption of fluoride, and after regeneration are shown in Figure 4. The spectrum demonstrate notable peak intensities at around 2Θ = 23.78 for 233, 26.46 for 312, 29.62 for 289, 32.72 for 447, 40.34 for 178, 47.36 for 173, 49.64 for 154, and 53.62 for 158, indicating that hydroxyapatite is present in the sample (Mohan & Dutta, 2020). There was a little drop in peak intensity following fluoride adsorption. The creation of calcium fluorite is indicated by the measured peaks at around 2Θ = 28.14 for 175, 46.80 for 160, and 55.31 for 87. (Poinern et al., 2011). Whereas the peaks at 2Θ = 28.90 for 132, 31.82 for 309, 39.54 for 154, 43.54 for 122, and 56.18 for 87 show the production of fluorapatite (Poinern et al., 2011). The peaks of the maize starch binder may be found at 2Θ = 22.04 for 219, 15.02 for 214, and 17.02 for 215. The presence of amorphous aluminium hydroxide was confirmed by the multiple weak diffraction peaks (Y.-X. Zhang & Jia, 2016).

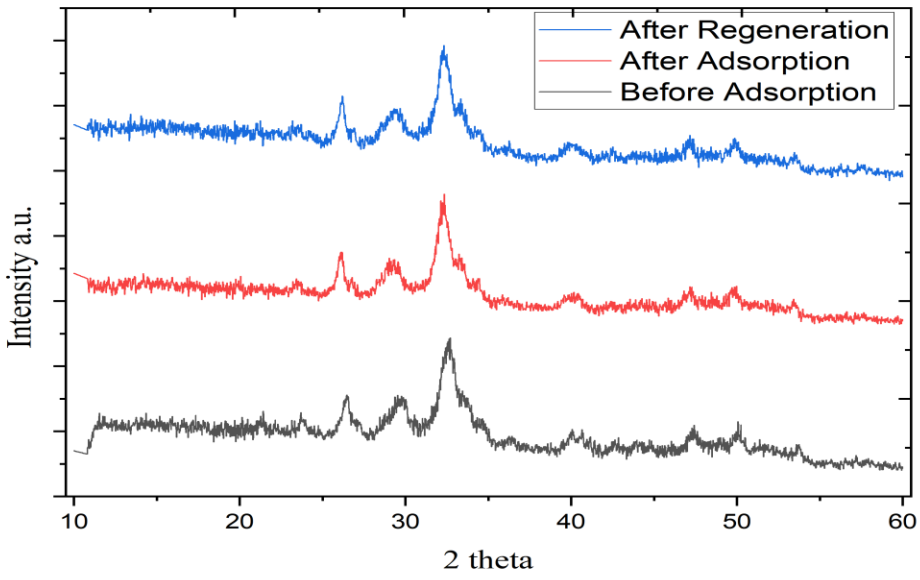

Figure 4: XRD spectra for Al(OH)3/HAP pellets for before adsorption, after adsorption and after regeneration

4.1.4 SEM characterization

The surface morphology of $Al(OH)_3$/HAP adsorbent pellets was characterized using scanning electron microscopy before and after adsorption, and after regeneration at 3000× magnification and 10000× magnification before adsorption to have a closer view, Figure 5 b. The unutilized pellets had an extremely uneven surface with lots of crevices that might be used to hold fluoride

ions, Figure 5a. The adsorbent showed signs of porosity before adsorption. Following fluoride adsorption, Figure 5c, the adsorbent exhibited filled pores and fluoride ions attached to the adsorbent surface. After regeneration, in Figure 5d, a reduction in the quantity of pores was observable in comparison to the unused adsorbent, which explains why the adsorption capacity dropped following each round of regeneration. Nevertheless, the adsorbent had a permeable consistency that suggested it could be reused.

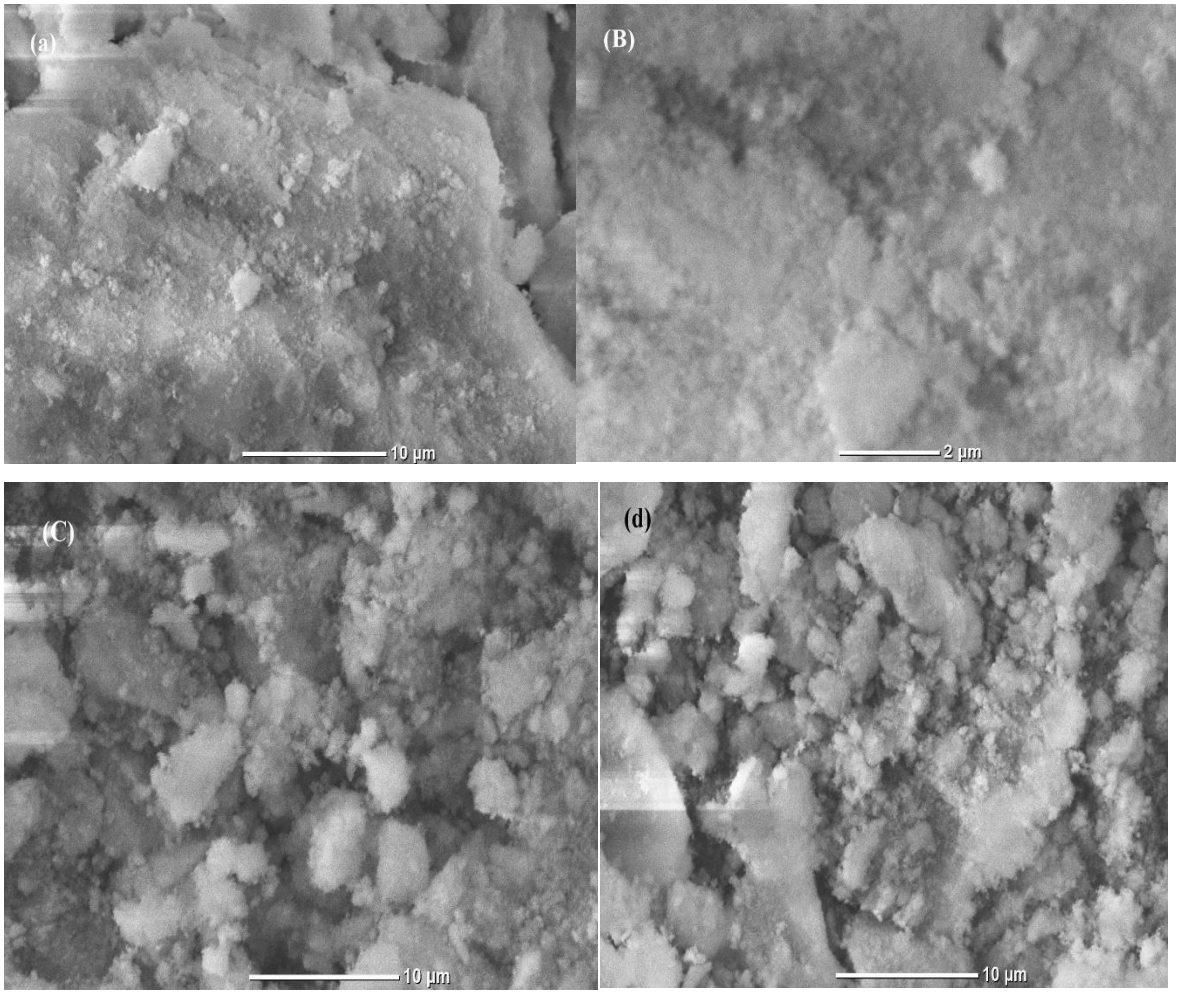

Figure 5:SEM of $Al(OH)_3$/HAP composite adsorbent pellets for (a) before adsorption (3000× magnification),(b)beforeadsorption(10,000×magnification),(c)Afteradsorption(3000×magnification), and (d) After regeneration(3000×magnification)

4.1.5 Drop Test and Water stability test results

To investigate the impact of binder ratios on the pellets strength, and their stability in aqueous solution, different amounts of bentonite and corn-starch were added to Aluminum hydroxide /HAP composite adsorbent to determine the optimal ratio. Four batches of pellets were produced with each type of binder, including pellets without binders, 5wt% binder, 10 wt.%,

and 15 wt.%. The literature was used to determine this range of binders because it is the most preferred range for pelletizing adsorbent (Bazer-Bachi et al., 2016).

It was observed, as seen in Figure (6), that the average drop number of pellets rose together with the amount of binder. Pellets containing a bentonite binder had resisted the most amount of drops. The pellets containing 5% corn starch were deemed inappropriate for the procedure because they failed to meet the required four drops, figure (6). Thus, by soaking the pellets in aqueous water containing 10 mg/l fluoride, the 10%, 15% corn-starch binder and the 5%, 10%, and 15% bentonite binder pellets were further examined. When the pellets containing 10% and 15% bentonite binder came into contact with aqueous water, they disintegrated completely, Appendix Figure 14. In a water-rich environment, bentonite absorbs water and works with the water to form cohesive forces between the particles that form pellets; however, it diminishes the porosity (Jo et al., 2021) and as the amount of bentonite binder increases the adsorbent pores spaces become more filled and internal cohesion of pellets weaken and eventually disintegrated due to combined effects of swelling induced pressure and decreased porosity the adsorbent pores (Y. Wan et al., 2020).

Following a 24-hour exposure to 10 mg/l fluoride, the pellets containing 10% and 15% corn-starch maintained their structural integrity, demonstrating that the integrity of the pellets was not compromised by the fluoride adsorption process. Research from the literature indicates that adding more binder reduces the surface area as it alters the adsorption properties by blocking the adsorbent's pores and occupying the active sites (Asgar Pour et al., 2023), Therefore, in light of this, it was determined that a 10% corn-starch binder and a 5% bentonite binder would be the best binder ratios as they showed stability in aqueous conditions and passed the drop tests. As a result, these samples were further selected to run additional tests.

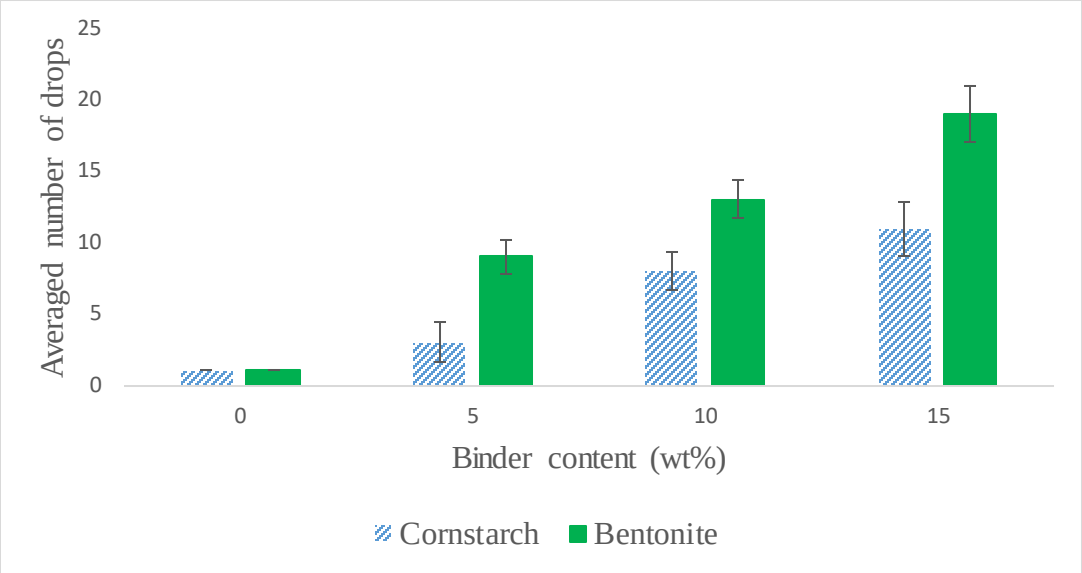

Figure 6: Strength test for $Al(OH)_3$/HAP pellets using drop test

4.2 Adsorption Experiment

4.2.1 Effects of Shape of Pellets

The impact shape of pellets on the effectiveness of fluoride removal was examined. in a continuous column experiment using cylindrical-shaped pellets of 5 mm in diameter and 1mm in length and Spherical pellets of 5mm in diameter. The initial fluoride concentration, bed depth, and flow rate were all maintained at 15 mg/l, 10 cm, and 15 ml/min, respectively. For cylindrical pellets, the bed mass was 37.134 grams, while for spherical pellets, it was 36.92 grams. With corresponding adsorption capacities of 1.34 mg/g and 0.679 mg/g, the breakthrough curves obtained are shown in Figure 7 a, below. Figure 7a demonstrated that the cylindrical pellets were more effective in removing fluoride than the spherical pellets. The breakthrough and exhaustion time for cylindrical shapes was delayed up to 2 hours and 9 hours respectively. The reason behind the delayed breakthrough and exhaustion time with cylindrical-shaped pellets could be that these forms have a high concentration of interparticle and intraparticle pores, along with a limited variation of pore diameters in the mesoporous area, which considerably enhances adsorption. Spherical-shaped pellets had a faster breakthrough which occurred at 30 mins and exhausted earlier compared with cylindrical pellets. This lower performance of the spherical shape could be due to its tight and dense structure which minimizes the void spaces between their particles reducing the pore volume and porosity hence lowering the surface area for adsorption. Comparable results were also reported by (Dou et al., 2013) regarding continuous column experiments investigating the effectiveness of different

adsorbent shapes in contaminant adsorption. Thus, for additional studies, cylindrical pellets were utilized.

4.2.2 Effects of Type of Binder

The effects of the type of binder in removing fluorides were investigated in a continuous column. The initial concentration of 10 mg/l, the flow rate of 15 ml/min, and the bed depth of 10 cm were maintained. The bed mass for pellets with corn-starch and bentonite binder was 37.134g and 37.104 g respectively. The breakthrough curves obtained in Fig 7 b, showed that the pellets with corn-starch binder were more effective in fluoride removal than pellets with bentonite binder. The adsorption capacity at breakthrough for pellets with corn-starch binder was 1.34 mg/g while the adsorption capacity of pellets with bentonite binder was 0.562 mg/g. The breakthrough time (t_b) of pellets with corn-starch and bentonite binder was 120 mins and 45 minutes respectively while the exhaustion time (t_e) was 9 h and 5 h respectively. This better performance of pellets with corn-starch binder than the pellets with bentonite binder could be because of the properties of the binder. When used as a binder, bentonite strengthens the pellets and lessens the fluoride adsorption sites as it blocks the surface of the adsorbent major fluoride adsorption sites. (Jo et al., 2021) reported comparable results of a reduction in the adsorbent's ability to absorb while using bentonite binder. Therefore, for further investigations cylindrical pellets formed using corn-starch binder was selected.

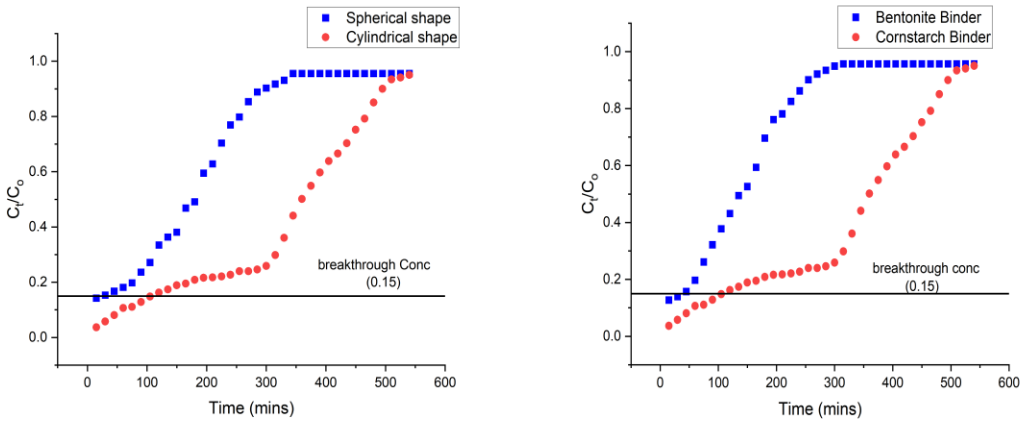

(a) (b)

Figure 7:Breakthrough curves for (a) Effect of Shape, and (b) Effect of type of binder

4.2.3 Effect of Flow Rate

The impact of flow rate on fluoride adsorption of $Al(OH)_3$/HAP pellets was investigated by varying flow rates at 15, 20, and 25 ml/min, while maintaining the initial concentration of fluoride at10 mg/l and bed mass of 37.134 grams (10 cm bed depth). The amount of effluent treated at a breakpoint for 15, 20, and 25 ml/min was 1.8 L, 1.5 L, and 1.125L respectively while at exhaustion points was 8.1 L, 7.8 L, and 6.375 L respectively Figure 8 a. It was also observed that as the rate of flow rose, there was a gradual rise in the steepness of the breakthrough curve. This might be because at a high flow rate, the interaction of fluoride ions with the adsorbent reduced hence fewer fluoride ions were adsorbed consequently diminishing the adsorption efficiency. Additionally, it could be because, at a higher flow rate, limited fluoride ion removal occurred as the fluoride ions left the column before adsorption achieved equilibrium (Geleta et al., 2021a). The mass transfer zone further supports this as it rose from 7.8cm to 8.23cm as the flow rate increased from 15 ml/min to 25 ml/min, table 5. As a result, at these flow rates, the adsorption capacity dropped from 1.34 mg/g to 0.792 mg/l**.** A decrease in empty bed contact time was also observed as shown in Table 6 below. Fluoride ions can access more active sites within the adsorbent at low flow rates because they have more time to come into contact with the adsorbate. Other researchers have also reported comparable observations (Geleta et al., 2021a; Mohan & Dutta, 2020; Y. Zhang et al., 2019).

Therefore, except for the impacts of flow rate, all experiments were conducted at the lowest flow rate of 15 ml/min since the greatest performance was noted at this rate.

4.2.4 Effect of Bed Height

To examine the impact of bed height, a column with varying bed heights of 5, 7.5, and 10 cm was pumped with an influent of 10 mg/l at a flow rate of 15 ml/min. The breakthrough curve obtained is illustrated in Figure 8 b. The bed mass at 5 cm, 7.5 cm, and 10cm was 20.37 g, 26.00g, and 37.134g respectively. The breakthrough time was 45 mins,75 minutes, and 120 mins for bed depths of 5, 7.5, and 10 cm respectively the exhaustion time also increased from 240 mins to 540 mins, and consequently, the total volume treated also increased from 3.6 l to 8.1 L as bed height increased from 5 cm to 10 cm respectively. The corresponding adsorption capacities were 0.89 mg/g, 1.04 mg/l, and 1.34 mg/l. This is due to the influent's longer residency duration in the column as bed depth increases, allowing for longer contact times and enough time for the adsorbates to diffuse into the adsorbent. The higher the bed height the higher the adsorption capacity. This observation agrees with other reported results in the

literature (Mehta et al., 2023; Mondal et al., 2018). Therefore, the bed height of 10 cm was used for all experiments except for the effect of bed height.

4.2.5 Effect of Initial Fluoride Concentration

A continuous column experiment was used to determine the impact of initial fluoride concentration on breakthrough with varying initial fluoride concentrations of 5, 10, and 15 mg/l. The flow rate and bed height were kept constant at 15 ml/min and 10 cm respectively. The breakthrough curves obtained in Figure 8 c, show that the gradient and the shape of breakthrough curves steepened as the fluoride concentration increased from 5 mg/l to 15 mg/l. The breakthrough time for 5 mg/l, 10 mg/l, and 15 mg/l was 150 minutes, 120 minutes, and 75 minutes respectively with corresponding adsorption capacities of 1.41mg/g, 1.34 mg/g, and 0.99mg/g. The reason for this trend is that the adsorbent's active sites are rapidly depleted because of the faster mass transfer of fluorides resulting from a higher concentration difference between the fluoride ions and the Al $(OH)_3$/HAP pellets adsorbent at higher fluoride concentrations. Additionally, it could be because the rise in fluoride concentration caused mass transfer resistance to decrease (Abdolali et al., 2017). Studies in literature have reported similar results for instance (Mohan & Dutta, 2020) in their assessment of the performance of continuous fixed-bed columns in fluoride removal using limestone coated with hydroxyapatite.

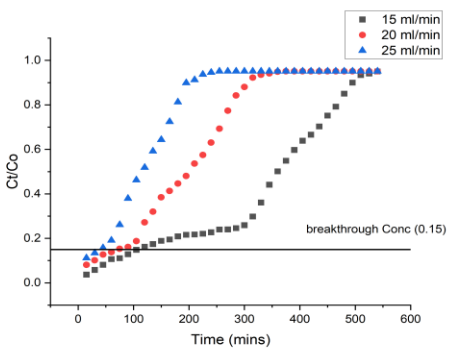

(a)

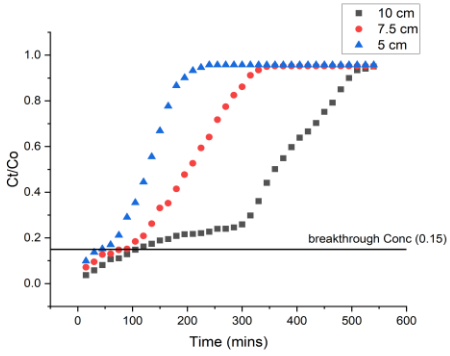

(b)

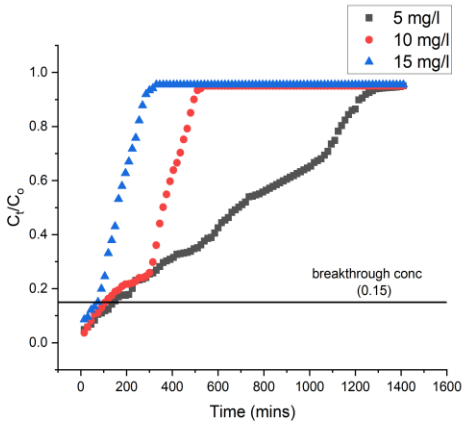

(c)

Figure 8: Breakthrough curves for varying process conditions (a) Effects of flow rate, (b) Effect of bed height, (c) Effect of initial concentration of fluoride

Table 5: Continuous column data obtained for fluoride removal using $Al(OH)_3$/HAP composite adsorbent pellets

parameters	Flow rate (ml/min)			Bed height (cm)			Initial Fluoride conc (mg/l)		
	15	20	25	5	7.5	10	5	10	15
t_b (mins)	120	75	45	45	90	120	150	120	75
t_e (mins)	540	375	255	240	360	540	1410	540	330
V_b (ml)	1800	1500	1125	675	1350	1800	2250	1800	1125
V_e (ml)	8100	7500	6375	3600	5400	8100	21150	8100	4950
MTZ (cm)	7.8	8	8.2	4.06	5.6	7.8	9	7.8	7.7
EBCT (mins)	6.06	4.5	3.6	3.03	4.5	6.06	6.06	6.06	6.06
Q_b (mg/g)	1.34	1.02	0.79	0.89	1.04	1.34	1.41	1.34	0.99

4.3 Central Composite Design

The height of the bed, initial concentration of fluorides, and rate of flow were the independent parameters in the statistical design, and the adsorption capacity was the response. The study employed a variety of tests, including the residual plots to ensure that the model was appropriate for approximation, analysis of variance (ANOVA) to ascertain the statistical relevance of the equation, and model fit summary to assess whether the model is applicable or not.

4.3.1 Model Fit Summary

Table 6, presents the statistical summary of the model, the cubic model was the aliased model. Based on the model with the highest order polynomial, the software proposed a quadratic model

whose additional terms were significant and the model did not alias Table 6. The quadratic model had the highest predicted and adjusted R-squared values. R-squared for the adsorption capacity regression model was 0.9722, Table 7, this high R-squared value indicated a significant association between the response variable and the independent variables since the majority of the variability (97 percent) in the adsorption capacity could be accounted for by the independent variables. Therefore, a quadratic model was used.

Table 6: Sequential model sum of squares

Source	Sum of Squares	DF	Mean Square	F Value	Prob > F	
Mean	13.71	1	13.71			
Linear	0.92	3	0.31	24.86	< 0.0001	
2FI	0.10	3	0.034	4.69	0.0198	
Quadratic	0.064	3	0.021	6.85	0.0087	Suggested
Cubic	0.011	4	2.659E- 003	0.78	0.5752	Aliased
Residual	0.020	6	3.394E-003			
Total	14.83	20	0.74			

Table 7:Model Summary Statistics

Source	Std. Dev.	R-Squared	Adjusted R-Squared	Predicted R-Squared	PRESS	
Linear	0.11	0.8234	0.7903	0.6822	0.36	
2FI	0.085	0.9151	0.8760	0.8237	0.20	
Quadratic	0.056	0.9722	0.9472	0.8369	0.18	Suggested
Cubic	0.058	0.9818	0.9422	-1.3362	2.61	Aliased

4.3.2 Analysis of Variance

Analysis of variance (ANOVA) results from Table 8 revealed the significance of the model with the F-value of 38.89 and the likelihood of a "model F-value" this high occurring as a result of noise was barely 0.01 percent.

According to Table (8), the lack of fit F-value of 2.61 suggested that the lack of fit was not statistically relevant in relation to the pure error. A strong lack of fit F-value had a 15.81 percent probability of being the result of noise. The model appeared to fit well, as indicated by the non-significant lack of fit being good. The adjusted R-squared of 0.9472, Table (9), and the predicted R-squared of 0.8369 had a difference of less than 0.2, indicating reasonable agreement.

The developed model was validated by the derived model's "Adequate precision" of 26.015, where a ratio of more than four indicates a desirable signal-to-noise ratio. It is therefore useful for navigating the design area.

Reproducible responses are those that do not surpass a 10 percent coefficient of variance (Cv), which is calculated by taking the estimate's standard error and dividing it by the observed response mean (Xiao et al., 2013). Therefore, Fluoride adsorption is guaranteed to be reproducible in the study because of the obtained C.V value of 6.7% (Table 9).

Based on the analysis of the software, the quadratic model was demonstrated to be the most appropriate when it came to the correlation between the response variable, y, and the independent variables, flow rate A, bed height B, and initial fluoride concentration C, Table 7. The regression coefficients of the response according to Equation (12) are represented in the following expression in terms of the coded factors equation (15).

$$Adsorption\ Capacity = +0.85 - 0.18A + 0.18B - 0.050C - 0.060C^2 + 0.064AC - 0.088BC \quad (15)$$

Significant model terms with "Prob> F" values less than 0.05 were A, B, C, C^2, AC, and BC, Table 8. When a value was greater than 0.100, it meant that the model terms were irrelevant and hence were not included in the model. Therefore, A^2, B^2, and AB were insignificant model terms, Table 8.

Table 8 Analysis of variance for Response Surface Quadratic Model

Source	Squares	DF	Sum of Square	Mean Value	F Prob > F	
Model	1.09	9	0.12	38.89	< 0.0001	significant
A	0.46	1	0.46	148.16	< 0.0001	
B	0.43	1	0.43	137.19	< 0.0001	
C	0.034	1	0.034	11.08	0.0076	
A^2	7.433E-003	1	7.433E-003	2.40	0.1525	
B^2	1.049E-006	1	1.049E-006	3.382E-004	0.9857	
C^2	0.052	1	0.052	16.65	0.0022	
AB	7.381E-003	1	7.381E-003	2.38	0.1538	
AC	0.033	1	0.033	10.61	0.0086	
BC	0.062	1	0.062	20.04	0.0012	
Residual	0.031	10	3.100E-003			
Lack of Fit	0.022	5	4.482E-003	2.61	0.1581	not significant
Pure Error	8.591E-003	5	1.718E-003			
Cor Total	1.12	19				

Table 8: Lack of fit statistics

Std. Dev.	0.056	R-Squared	0.9722
Mean	0.83	Adj R-Squared	0.9472
C.V.	6.72	Pred R-Squared	0.8369
PRESS	0.18	Adeq Precision	26.015

4.3.3 Residual Plots.

To make sure that the model was suitable for approximation, the residual plots were utilized to verify its appropriateness. To ascertain whether or not the residuals followed a normal distribution, a plot of the normal percent probability versus studentized for fluoride adsorption by $Al(OH)_3$/HAP pellets was employed in Figure 9(a) and it indicated that fluoride adsorption study by $Al(OH)_3$/HAP pellets largely satisfied the normality assumption since the dots in the plots created a rather straight line, indicating that the normal distribution of that data set was closely obtained. The Studentized residuals quantify the number of standard deviations between the residual and predicted values (Figure 9b). They are calculated by dividing the residuals by that residual's estimated standard deviation (Baharlouei et al., 2018) and plot of residuals versus predicted lied between the +3 and -3 range (Figure 9b), further confirming that the adsorption process satisfied the normality assumption. Figure 9 (c) shows a plot of studentized residual versus run, a random scatter was obtained between +3 and -3. It is evident from Figure 9(d) below that the surface model was effective in obtaining the relationship between the variables impacting the quantity of fluorides adsorbed because the projected values produced were extremely close to the experimental values.

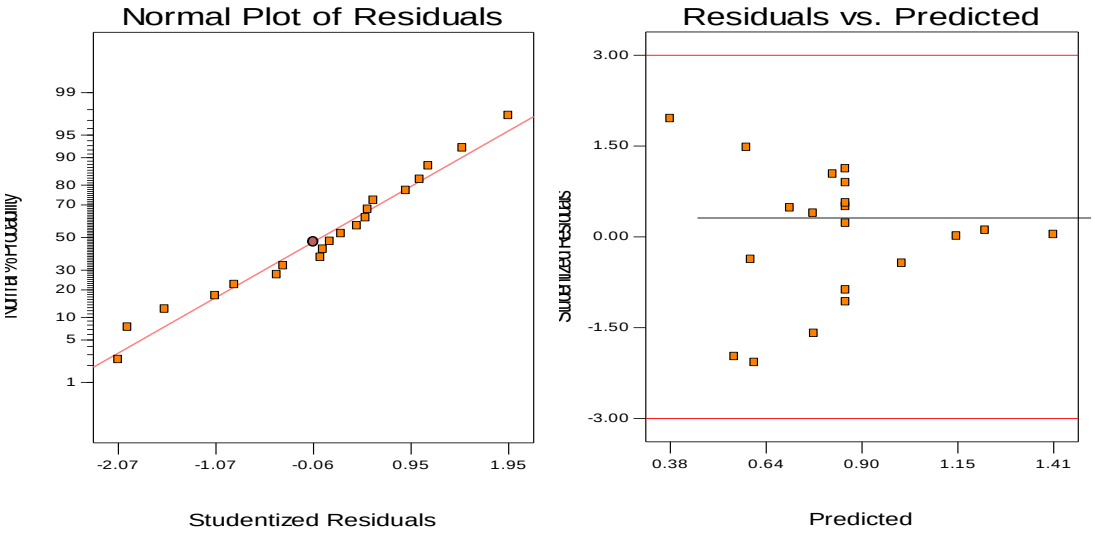

(a) (b)

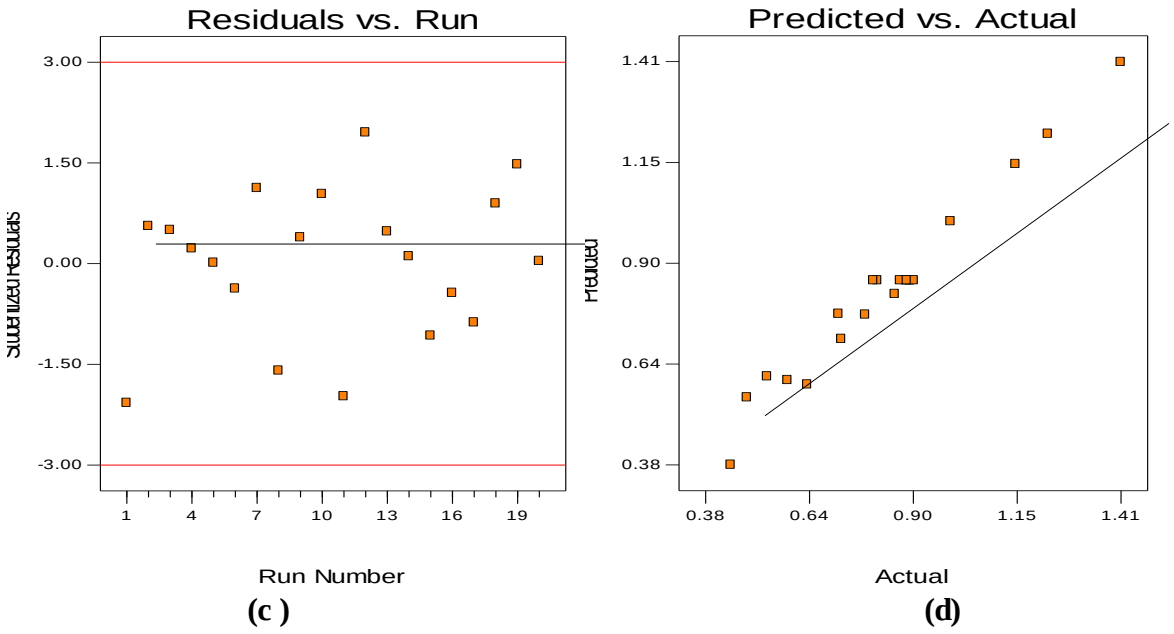

Figure 9: Diagnostic plots for (a) normal % probability versus studentized, (b) predicted and residuals values, (c) Residuals versus run, and (d) predicted versus actual

4.3.4 Response Surface Optimization

The desirability function was used to optimize fluoride adsorption by $Al(OH)_3$/HAP pellets numerically. Maximizing the adsorption capacity was the chosen objective for the optimization of fluoride adsorption by $Al(OH)_3$/HAP pellets. As a result, the ranges under investigation were chosen for the independent variable values, and the intended criteria for fluoride adsorption were established at their highest value.

There were nine distinct solutions, each with varying levels of independent variables. The optimal fluoride adsorption conditions were determined by choosing the solution that yielded the maximum desirability. The desirability function's value of 0.99 indicates that the expected value might accurately reflect the experimental model. The model projected an optimal response adsorption capacity of 1.40 mg/g with a bed height of 10 cm, initial fluoride concentration of 5.00, and a flow rate of 15 ml/min. A real experiment in the process settings was conducted to evaluate the process's optimum conditions further, and the findings presented in Table (10) indicated that the optimization by response surface model agreed well with the experimental verification.

Table 9:Verification experiment results of the model under optimized conditions

Run	flow rate (A)(ml/min)	bed height (B) (cm)	initial fluoride concentration (mg/l)	Adsorption Capacity (mg/g)		
				experimental	predicted	error(%)
1	15	10	5	1.41	1.40	1

4.4 Modelling Breakthrough Curves

Table 11 below shows the calculated parameters of the Yoon Nelson model, Adam and Bohart Model, and Thomas model when process parameters were varied that is the flow rate, bed height, and initial ion concentration. The slope and intercept of the models' linear plots were used to compute the parameters. The R^2 for the Adams-Bohart model as shown in the table below was 0.91-0.95 for flow rate,0.89-0.92 for Initial fluoride concentration, and 0.95-0.96 for bed heights. The R^2 for the Thomas model was 0.92-0.99 for flow rates, 0.92-0.99 for initial concentration and 0.92-0.98 for bed heights, and finally, the Yoon –Nelson R^2 was 0.92-0.99 for flow rates, 0.92-0.99 for initial fluoride concentration and 0.92-0.98 for bed height. The highest R^2 values were obtained with the Thomas model and Yoon-Nelson for all process parameters demonstrating the models' suitability for the adsorption of fluoride ions by $Al(OH)_3$ /HAP pellets.

Table 10:Adam-Bohart, Thomas, and Yoon-Nelson Model parameters for continuous column fluoride removal by $Al(OH)_3$/HAP pellets

Adsorption parameters		Adams Bohart Model				Thomas model			Yoon-Nelson model		
		K_{AB} (L/mg.min) $*10^{-4}$	N_o (mg/l)	F (cm/min)	R^2	K_{Th} (L/mg.min $*10^{-4}$)	Q_0 (mg/g)	R^2	K_{YN} (min^{-1})$*10^{-3}$	τ (mins)	R^2
Flow Rate (ml/min)	15	5.22	845.6	1.65	0.95	9.79	1.32	0.92	9.79	327	0.92
	20	7.04	715	2.20	0.94	15.82	0.989	0.98	15.82	184	0.98
	25	9.42	599.6	2.75	0.91	22.91	0.774	0.99	22.91	115	0.99
Initial Fluoride Concentration (mg/l)	5	3.24	1030.6	1.65	0.89	7.1	1.38	0.96	3.55	681	0.96
	10	5.22	845.6	1.65	0.95	9.79	1.32	0.92	9.79	327	0.92
	15	5.413	704	1.65	0.92	11.87	0.983	0.99	17.81	162	0.99
Bed height (cm)	5	10.89	690.7	1.65	0.95	25.51	0.858	0.98	25.51	117	0.98
	7.5	7.68	699.7	1.65	0.96	16.28	1.08	0.98	16.28	188	0.98
	10	5.22	845.6	1.65	0.95	9.79	1.32	0.92	9.79	327	0.92

4.4.1 Adams-Bohart Model

The Adams-Bohart model was used to describe the initial part of breakthrough curve characteristics parameters that is the kinetic constant (K_{AB}) and maximal adsorption capacity (No) obtained from linear plots of ln(Ct/Co) versus t, Appendix Figure 15. From Table 11, as may be observed, the R^2 coefficients of determination fell between 0.89 and 0.96. When flow rates and initial fluoride concentration increased, the values of N_o declined but increased with bed height which explains the adsorption capabilities of the adsorbent at high bed heights due to an increase in the amount of active sites. It was observed that the kinetic constant rose as the flow rate increased. Thus, the external mass transfer in the column fluoride adsorption process dominates the changes in the system as a whole (Quintelas et al., 2013; Salifu, 2017). This is in line with the findings published in the literature (Geleta et al., 2021b).

4.4.2 Thomas Model

The various parameters of the Thomas model, R^2, the rate constant (K), maximum solid phase concentration of fluoride ions, Q_o (mg/g) were calculated from the linear plots of ln [(Co/Ct) - 1] verses t at different process conditions Appendix Fig 16. The model demonstrated a good description of the continuous process of fluoride adsorption by $Al(OH)_3$/HAP pellets in continuous columns, as evidenced by its high R^2 value, which ranged from 0.91-0.99. From the analysis of the results obtained, in Table 11, It was noted that K_T values dropped with increasing bed height but showed a rising tendency with an increase in flow rate. Q_o dropped when flow rates increased due to a shorter interaction time between the fluoride ions and adsorption sites; however, it increased as bed height increased because the fluoride ions had a longer contact time with the adsorbent (Ghosh et al., 2014, 2015).To sum up, while the values of the maximum solid phase concentration reduce, the Thomas rate constant increases with the flow rate. This is consistent with the findings described in the literature (Geleta et al., 2021b; Yagub et al., 2015). The experimental data's Qo values were discovered to be extremely near to the anticipated values, indicating the validity of the model.

4.4.3 Yoon-Nelson Model

The Yoon-Nelson parameters were obtained from the linear plots of ln [Ct/(Co-Ct)] versus t as shown in Appendix Figure 17. From Table 11 it can be observed that the R^2 was between 0.92 –0.99. The K_{YN} values increased while τ decreased with both a rise in flow rate and initial concentration of fluoride concentration due to the adsorbent quickly reaching saturation at greater concentration. Conversely, as the bed height increased, the τ, values increased while the K_{YN} values decreased this is in line with the findings published in the literature (Abu Bakar et al., 2019; Bishayee et al., 2022)(Mohan & Dutta, 2020). The maximum time required for 50 percent of adsorbate to a breakthrough was 327 minutes at a bed height of 10cm, 10 mg/l fluoride contents, and 15 ml/min flow rate (table 11).

4.4.4 Bed Depth Service Time (BDST) Model

The parameters for the BDST model Table 12 were obtained from a slope and intercept of the Appendix Figure 18. According to the R^2 value of 0.987, the model was found to be valid and to be able to forecast the service time of $Al(OH)_3$/HAP pellets as well as the effectiveness of the pellets bed in removing fluoride. It was also noted that when bed height increased, breakthrough and exhaustion times increased as well. This was because there was more adsorbent in the column, which extended the adsorbent's service life. This compares favorably

to the findings reported by (Kumari et al., 2021; Talat et al., 2018). The column's critical bed depth (H_o), as determined from Equation 5, was 1.8 cm. The BDST model constants (N_0, and K_α) can be valuable in scaling up the procedure for varying fluoride concentrations and flow rates without necessitating further experimental runs.

Table 11: Bed depth service time (BDST) model parameters for Al(OH)3/HAP pellets fluoride adsorption (C0= 10mg/l, Q=15ml/min)

C_t/C_o	Slope (a)	Intercept (b)	N_0 (mg/l)	K_α (L/mg/min)	R^2
0.15	15	-27.5	247.5	0.00631	0.987
0.95	60	-70	990	0.00421	0.987

4.5 Reusability of Adsorbent

In three cycles of adsorption and desorption, the reusability of the adsorbent was assessed, (Figure 10). The pellets exhibit good reusability for fluoride ions when desorption with 10% caustic soda is carried out for up to three cycles, as shown in Figure 10 below. To reduce the amount of eluent needed for the desorption of fluoride ions, the lowest flow rate of 15 ml/min was employed. It was observed that the adsorption capacity dropped from 1.11mg/g, 0.977, and 0.955 during the first, second, and third cycles respectively, and consequently the desorption efficiency from 88 %, 71%, and 61% by the third cycle this could be because fluoride ions may have saturated the active sites since the regeneration was only done until the concentration was below 0.15 mg/l meaning some fluorides remained in the adsorbent. First, 3.8 liters of eluent were used; in the last cycle, that amount was lowered to two liters which was because of decreasing adsorption of adsorbent. There was not much difference between the 2ndcycle's adsorption and the third cycle meaning the adsorption can be further regeneration for other cycles beyond the three cycles indicating the efficiency of 10 % sodium hydroxide eluent.

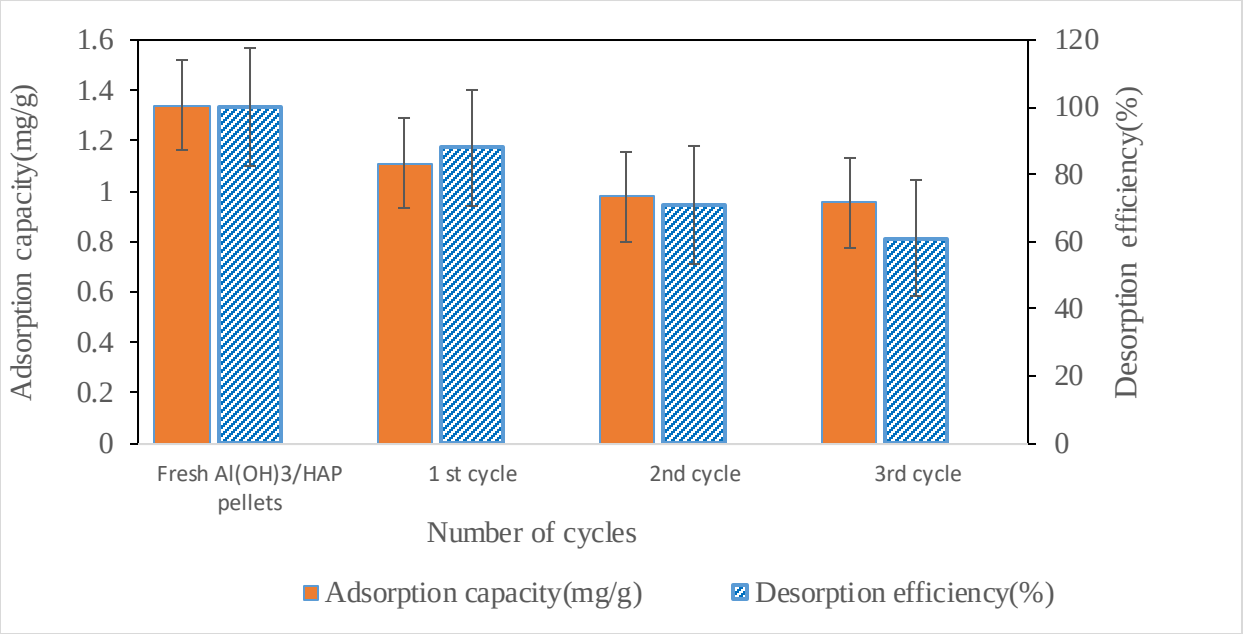

Figure 10:Regeneration of $Al(OH)_3$/HAP pellets Adsorbent in Adsorption-Desorption Cycles

4.6 Comparison of $Al(OH)_3$/HAP Pellets with other Adsorbents in Continuous Column Defluoridation

The table below compares the current adsorbent with other reported adsorbents in the literature based on their adsorption capabilities. With the adsorption capacity of 1.34 mg/g, the present adsorbent was found better than the powder form of the adsorbent form due to the presence of extra hydroxyl groups in the pellets from the addition of corn-starch binder. The gelatinization process of the binder caused the dispersion of starch molecules in water and the disruption of their granule structure enhancing the hydroxyl groups' availability and accessibility. Consequently, the addition of starch gel as a binder to the composite with the more accessible -OH groups may have provided extra sites for adsorption which would have improved the performance of the pellets when compared to the powder form. A similar observation of improved adsorption capacity of shaped adsorbents as compared to their powder form was also reported in the literature by (Laonapakul et al., 2022). Also the fact that powders tend to agglomerate easily during the adsorption process due to their nature as particles may also contribute to the superior adsorption of pellets over powder. This phenomenon reduces the effective surface area available for adsorption by creating areas that are inaccessible to fluoride-contaminated water (Lou et al., 2022). The adsorbent also performed better than some of the adsorbents such as Synthesized marble hydroxyapatite pellets and Hydrous Ferric oxide. The initial concentration of fluoride ions and the adsorption capacities of the adsorbents were used as a basis of comparison.

Table 12:Comparison of performance $Al(OH)_3$/HAP with other Adsorbents in column defluoridation

Adsorbent	Process condition			Adsorption Capacity (mg/g)	Reference
	Bed height (cm)	Initial concentration (mg/l)	Flow Rate (ml/min)		
Synthesized marble hydroxyapatite pellets	25	10	0.0166	1.21	(Mehta et al., 2023)
Magnesium-Incorporated Hydroxyapatite pellets	30	10	0.0166	1.46	(Mondal et al., 2018)
Hydrous Ferric Oxide	12	10	0.042	1.19	(Nur et al., 2014)
Aluminum-Modified Hematite	2.5	10	1	2.37	(Teutli-Sequeira et al., 2015)
Aluminum-Modified Zeolitic Tuff	4	10	1	3.24	(Teutli-Sequeira et al., 2015)
Aluminium hydroxide/Hap powder	10	10	15	1.28	(Opoka et al., 2023)
Aluminum hydroxide/Hap pellets	10	10	15	1.34	**Current Study**

4.7 Fluoride Removal from Groundwater

The performance of $Al(OH)_3$/HAP pellets in fluoride removal from groundwater was evaluated. The water quality of the treated groundwater samples was analyzed and reported in Table 13 below. The initial fluoride concentration was 10.7 mg/l. The optimum conditions of a 15 ml/min flow rate and a bed height of 10 cm were used to treat the groundwater in a continuous column experiment and it was observed that the concentration of 1.5 mg/l, the World Health recommended limit of fluoride in drinking water was reached at 75 minutes which was too soon as compared to the laboratory testing with synthetic water with concentration of 10 mg/l this might be due to presence of many cations which may cause the shortened the breakthrough time and the complex matrix of groundwater could have obstructed the fluoride removal .

Table 13:Treated Groundwater water quality parameters

Parameter	
pH	7.438
Electrical Conductivity (µs/cm)	1042
Fluoride (mg/l)	1.5
TDS (mg/l)	765
Total Alkalinity as $CaCO_3$ (mg/l)	494
Calcium (mg/l)	112
Aluminum (mg/l)	0.1
Phosphate (mg/l)	1.19

5.0 Conclusion and Recommendations

5.1 Conclusion

This study investigated the feasibility of utilization of structured Aluminium hydroxide/ hydroxyapatite composite adsorbent in fluoride removal from drinking water. The shaped composite adsorbent was fabricated into spherical and cylindrical shapes using locally made shaping equipment using bentonite and Corn starch binder and upon investigation in a continuous column experiment the research found out that cylindrical shape with corn-starch binder was effective for the investigation based on their performance in fluoride removal. Therefore, the research was carried out with cylindrical pellets with corn-starch binder.

The effects of process parameters flow rate, bed height, and initial fluoride concentration were investigated. It was noted that the highest bed height (10cm) combined with the lowest flow rate (15 ml/min) was the most effective condition for column defluoridation. These process parameters were further optimized with central composite statistical experimental design under Response surface methodology (RSM) and the experimental adsorption capacity of the adsorbent at optimized conditions (15 ml/min flow rate, 10cm bed height, and 5mg/l fluoride concentration) was 1.41 mg/g which was in close to the model prediction of 1.40 mg/g.

The column Adsorption breakthrough curves were fitted to kinetic models Adams Bohart, Yoon Nelson, and Thomas Model. The experimental data's Qo values were discovered to be extremely near to the anticipated values from Thomas's model fitting, indicating the validity of the model. Also, Yoon Nelson showed a good fit to the experimental data. The relationship between the breakthrough time and bed height was expressed using the BDST model. The achieved high R^2 value demonstrated the reliability of the model in its applicability in forecasting the time required for a breakthrough under different process circumstances.

The reusability of the adsorbent was investigated in three adsorption-desorption cycles with a desorption efficiency of 88% percent in the first cycle, 71 % in the second cycle, and 61 % by the third cycle as a result the adsorption capacity of 1.11 mg/g, 0.977 mg/g, 0.955 mg/g being achieved respectively indicating that the adsorbent can be reused.

The effectiveness of the pellets in fluoride removal was further investigated using raw water samples and the treated water was analyzed for various water quality parameters. It was observed the complex matrix of the groundwater interfered with fluoride removal but even so, the fluoride levels were successfully reduced to below the World Health Recommended limit of 1.5 mg/l.

5.2 Recommendations

Following the study's findings, which showed the efficacy and promise of $Al(OH)_3$/HAP composite adsorbent pellets for removing fluoride from drinking water, several suggestions are made to improve the effectiveness and practical applicability of these adsorbent. It is recommended to resynthesize the pellets with lower particle sizes since the adsorbent composite pellets were synthesized with 5 mm diameters. Smaller diameters, such as 2-3 mm, will optimize the surface area for fluoride adsorption, resulting in a better adsorption capacity. Adsorbent regeneration was limited to three cycles, and the regeneration efficiency was only 61% after those three cycles. Consequently, it is necessary to continue the adsorption-desorption cycles after the third cycle to assess long-term reusability and ascertain the greatest number of efficient regeneration cycles. It is imperative to investigate alternative binders to structure composite adsorbents. Additionally, alternative forms of the composite, such as granules, should be investigated. Additionally, it is recommended to evaluate the composite's long-term stability and performance under continuous use. This should entail researching extended exposure to natural water matrices, the possibility of fouling and mechanical wear on the adsorption capacity, and the adsorbent's structural integrity. Lastly, even though the pellets maintained their structural integrity throughout the adsorption process, further investigations on the mechanical strength of the adsorbent is recommended

References

Abdolali, A., Ngo, H. H., Guo, W., Zhou, J. L., Zhang, J., Liang, S., Chang, S. W., Nguyen, D. D., & Liu, Y. (2017). Application of a breakthrough biosorbent for removing heavy metals from synthetic and real wastewaters in a lab-scale continuous fixed-bed column. *Bioresource Technology*, *229*, 78–87.

Abifarin, J. K., Obada, D. O., Dauda, E. T., & Dodoo-Arhin, D. (2019). Experimental data on the characterization of hydroxyapatite synthesized from biowastes. *Data in Brief*, *26*, 104485. https://doi.org/https://doi.org/10.1016/j.dib.2019.104485

Abu Bakar, A. H., Abdullah, L. C., Mohd Zahri, N. A., & Alkhatib, M. (2019). Column efficiency of fluoride removal using Quaternized Palm Kernel Shell (QPKS). *International Journal of Chemical Engineering*, *2019*.

Ahmed, Y. M. Z., El-Sheikh, S. M., & Zaki, Z. I. (2015). Changes in hydroxyapatite powder properties via heat treatment. *Bulletin of Materials Science*, *38*, 1807–1819.

Alagumuthu, G., & Rajan, M. (2010). Equilibrium and kinetics of adsorption of fluoride onto zirconium impregnated cashew nut shell carbon. *Chemical Engineering Journal*, *158*(3), 451–457. https://doi.org/https://doi.org/10.1016/j.cej.2010.01.017

Ali, S., Thakur, S. K., Sarkar, A., & Shekhar, S. (2016). Worldwide contamination of water by fluoride. *Environmental Chemistry Letters*, *14*, 291–315.

Altufaily, M. A. M., AL-Mansori, N. J., & AL-Qaraghulee, A. F. M. (2019). Mathematical modeling of fixed-bed columns for the adsorption of methylene blue on to fired clay pot. *Int J ChemTech Res*, *12*, 70–80.

Anbia, M., & Aghaei, M. (2019). Study of the effect of organic binders on 13X zeolite agglomeration and their CO2 adsorption properties. *Scientia Iranica*, *26*(3), 1497–1504.

Ariffin, N., Abdullah, M. M. A. B., Postawa, P., Zamree Abd Rahim, S., Mohd Arif Zainol, M. R. R., Putra Jaya, R., Śliwa, A., Omar, M. F., Wysłocki, J. J., & Błoch, K. (2021). Effect of aluminium powder on kaolin-based geopolymer characteristic and removal of Cu2+. *Materials*, *14*(4), 814.

Arya, S., Subramani, T., Vennila, G., & Karunanidhi, D. (2021). Health risks associated with fluoride intake from rural drinking water supply and inverse mass balance modeling to decipher hydrogeochemical processes in Vattamalaikarai River basin, South India. *Environmental Geochemistry and Health*, *43*, 705–716.

Asgar Pour, Z., Abduljawad, M. M., Alassmy, Y. A., Cardon, L., Van Steenberge, P. H. M., & Sebakhy, K. O. (2023). A Comparative Review of Binder-Containing Extrusion and

Alternative Shaping Techniques for Structuring of Zeolites into Different Geometrical Bodies. *Catalysts*, *13*(4), 656.

Ashogbon, A. O., & Akintayo, E. T. (2014). Recent trend in the physical and chemical modification of starches from different botanical sources: A review. *Starch-Stärke*, *66*(1–2), 41–57.

Ashouri, V., Ghalkhani, M., Adib, K., & Rahimi Nasrabadi, M. (2022). Synthesis and shaping of Zr-UiO-66 MOF applicable as efficient phosalone adsorbent in real samples. *Polyhedron*, *215*, 115653. https://doi.org/https://doi.org/10.1016/j.poly.2022.115653

Azha, S. F., Shahadat, M., Ismail, S., Ali, S. W., & Ahammad, S. Z. (2021). Prospect of clay-based flexible adsorbent coatings as cleaner production technique in wastewater treatment, challenges, and issues: A review. *Journal of the Taiwan Institute of Chemical Engineers*, *120*, 178–206. https://doi.org/https://doi.org/10.1016/j.jtice.2021.03.018

Baharlouei, A., Jalilnejad, E., & Sirousazar, M. (2018). Fixed-bed column performance of methylene blue biosorption by Luffa cylindrica: statistical and mathematical modeling. *Chemical Engineering Communications*, *205*(11), 1537–1554.

Bazer-Bachi, D., Harbuzaru, B., & Lecolier, E. (2016). *Zeolite formed by extrusion and pelleting with a hydraulic binder having improved mechanical properties and process and preparing same*. Google Patents.

Bertolini, T. C. R., Fungaro, D. A., & Mahmoud, A. E. D. (2022). The influence of separately and combined bentonite and kaolinite as binders for pelletization of NaA zeolite from coal fly ash. *Cerâmica*, *68*, 375–384.

Bhatnagar, A., Kumar, E., & Sillanpää, M. (2011). Fluoride removal from water by adsorption—a review. *Chemical Engineering Journal*, *171*(3), 811–840.

Bishayee, B., Ruj, B., Nandi, S., Chatterjee, R. P., Mallick, A., Chakraborty, P., Nayak, J., & Chakrabortty, S. (2022). Sorptive elimination of fluoride from contaminated groundwater in a fixed bed column: A kinetic model validation based study. *Journal of the Indian Chemical Society*, *99*(1), 100302.

Bohart, G. S., & Adams, E. Q. (1920). SOME ASPECTS OF THE BEHAVIOR OF CHARCOAL WITH RESPECT TO CHLORINE.1. *Journal of the American Chemical Society*, *42*(3), 523–544. https://doi.org/10.1021/ja01448a018

Chanut, N., Wiersum, A. D., Lee, U., Hwang, Y. K., Ragon, F., Chevreau, H., Bourrelly, S., Kuchta, B., Chang, J., & Serre, C. (2016). Observing the effects of shaping on gas adsorption in metal-organic frameworks. *European Journal of Inorganic Chemistry*, *2016*(27), 4416–4423.

Chavali, R., Gunda, N. S. K., Naicker, S., & Mitra, S. K. (2015). Rapid detection of fluoride in potable water using a novel fluorogenic compound 7-O-tert-butyldiphenylsilyl-4-methylcoumarin. *Analytical Chemistry Research*, *6*, 26–31. https://doi.org/https://doi.org/10.1016/j.ancr.2015.10.003

Chen, I.-P., Kan, C.-C., Futalan, C. M., Calagui, M. J. C., Lin, S.-S., Tsai, W. C., & Wan, M.-W. (2015). Batch and fixed bed studies: Removal of copper (II) using chitosan-coated kaolinite beads from aqueous solution. *Sustainable Environment Research*, *25*(2).

Cho, D.-W., Han, Y.-S., Lee, J., Jang, J.-Y., Yim, G.-J., Cho, S., Lee, J.-S., & Cheong, Y.-W. (2020). Water defluorination using granular composite synthesized via hydrothermal treatment of polyaluminum chloride (PAC) sludge. *Chemosphere*, *247*, 125899.

Coelho, C. C., Grenho, L., Gomes, P. S., Quadros, P. A., & Fernandes, M. H. (2019). Nano-hydroxyapatite in oral care cosmetics: Characterization and cytotoxicity assessment. *Scientific Reports*, *9*(1), 11050.

Dang, X., Yu, Z., Yang, M., Woo, M. W., Song, Y., Wang, X., & Zhang, H. (2022). Sustainable electrochemical synthesis of natural starch-based biomass adsorbent with ultrahigh adsorption capacity for Cr (VI) and dyes removal. *Separation and Purification Technology*, *288*, 120668.

Dessalegne, M., Zewge, F., Pfenninger, N., Johnson, C. A., & Diaz, I. (2016). Layered double hydroxide and its calcined product for fluoride removal from groundwater of Ethiopian Rift Valley. *Water, Air, & Soil Pollution*, *227*, 1–13.

Dhillon, A., Prasad, S., & Kumar, D. (2017). Recent advances and spectroscopic perspectives in fluoride removal. *Applied Spectroscopy Reviews*, *52*(3), 175–230.

Dlamini, D. S., Tesha, J. M., Vilakati, G. D., Mamba, B. B., Mishra, A. K., Thwala, J. M., & Li, J. (2020). A critical review of selected membrane-and powder-based adsorbents for water treatment: Sustainability and effectiveness. *Journal of Cleaner Production*, *277*, 123497.

Dou, X., Mohan, D., & Pittman Jr, C. U. (2013). Arsenate adsorption on three types of granular schwertmannite. *Water Research*, *47*(9), 2938–2948.

Dou, X., Zhang, Y., Wang, H., Wang, T., & Wang, Y. (2011). Performance of granular zirconium–iron oxide in the removal of fluoride from drinking water. *Water Research*, *45*(12), 3571–3578. https://doi.org/https://doi.org/10.1016/j.watres.2011.04.002

Dragan, E. S., & Dinu, M. V. (2020). Advances in porous chitosan-based composite hydrogels: Synthesis and applications. *Reactive and Functional Polymers*, *146*, 104372.

Dubey, S., Agrawal, M., & Gupta, A. B. (2018). Advances in coagulation technique for

treatment of fluoride-contaminated water: a critical review. *Reviews in Chemical Engineering*, *35*(1), 109–137.

Elouahli, A., Zbair, M., Anfar, Z., Ahsaine, H. A., Khallok, H., Chourak, R., & Hatim, Z. (2018). Apatitic tricalcium phosphate powder: High sorption capacity of hexavalent chromium removal. *Surfaces and Interfaces*, *13*, 139–147. https://doi.org/https://doi.org/10.1016/j.surfin.2018.09.006

Fungaro, D. A., & Bertolini, T. (2022). Optimization of Pelleting Parameters for Producing Composite Pellets Using Zeolitic Material From Fly Ash. *Journal of Applied Materials and Technology*, *3*(2), 13–23.

Geleta, W. S., Alemayehu, E., & Lennartz, B. (2021a). Enhanced Defluoridation of Water Using Zirconium—Coated Pumice in Fixed-Bed Adsorption Columns. *Materials*, *14*(20), 6145.

Geleta, W. S., Alemayehu, E., & Lennartz, B. (2021b). Volcanic rock materials for defluoridation of water in fixed-bed column systems. *Molecules*, *26*(4), 977.

George, S., Mehta, D., & Saharan, V. K. (2020). Application of hydroxyapatite and its modified forms as adsorbents for water defluoridation: an insight into process synthesis. *Reviews in Chemical Engineering*, *36*(3), 369–400.

Gharsallaoui, A., Roudaut, G., Chambin, O., Voilley, A., & Saurel, R. (2007). Applications of spray-drying in microencapsulation of food ingredients: An overview. *Food Research International*, *40*(9), 1107–1121.

Ghosh, A., Chakrabarti, S., Biswas, K., & Ghosh, U. C. (2014). Agglomerated nanoparticles of hydrous Ce (IV)+ Zr (IV) mixed oxide: Preparation, characterization and physicochemical aspects on fluoride adsorption. *Applied Surface Science*, *307*, 665–676.

Ghosh, A., Chakrabarti, S., Biswas, K., & Ghosh, U. C. (2015). Column performances on fluoride removal by agglomerated Ce (IV)–Zr (IV) mixed oxide nanoparticles packed fixed-beds. *Journal of Environmental Chemical Engineering*, *3*(2), 653–661.

Golie, W. M., & Upadhyayula, S. (2016). Continuous fixed-bed column study for the removal of nitrate from water using chitosan/alumina composite. *Journal of Water Process Engineering*, *12*, 58–65.

Grzegorzek, M., & Majewska-Nowak, K. (2016). Use of the electrodialysis process for fluoride ion and salt removal from multi-constituent aqueous solutions. *Architecture, Civil Engineering, Environment*, *9*(4), 107–113.

Grzegorzek, M., Majewska-Nowak, K., & Ahmed, A. E. (2020). Removal of fluoride from multicomponent water solutions with the use of monovalent selective ion-exchange

membranes. *Science of the Total Environment*, *722*, 137681.

Guaya, D., Maza, L., Angamarca, A., Mendoza, E., García, L., Valderrama, C., & Cortina, J. L. (2022). Fe3+/Mn2+ (Oxy) Hydroxide Nanoparticles Loaded onto Muscovite/Zeolite Composites (Powder, Pellets and Monoliths): Phosphate Carriers from Urban Wastewater to Soil. *Nanomaterials*, *12*(21), 3848.

Gul, A., Sirkeci, A. A., Boylu, F., Guldan, G., & Burat, F. (2015). Improvement of mechanical strength of iron ore pellets using raw and activated bentonites as binders. *Physicochemical Problems of Mineral Processing*, *51*(1), 23–36.

Gwala, P., Andey, S., Mhaisalkar, V., Labhasetwar, P., Pimpalkar, S., & Kshirsagar, C. (2011). Lab scale study on electrocoagulation defluoridation process optimization along with aluminium leaching in the process and comparison with full scale plant operation. *Water Science and Technology*, *63*(12), 2788–2795.

Hernandez-Eudave, M. T., Bonilla-Petriciolet, A., Moreno-Virgen, M. R., Rojas-Mayorga, C. K., & Tovar-Gómez, R. (2016). Design analysis of fixed-bed synergic adsorption of heavy metals and acid blue 25 on activated carbon. *Desalination and Water Treatment*, *57*(21), 9824–9836.

Hong, H.-J., Park, I.-S., Ryu, T., Ryu, J., Kim, B.-G., & Chung, K.-S. (2013). Granulation of Li1.33Mn1.67O4 (LMO) through the use of cross-linked chitosan for the effective recovery of Li+ from seawater. *Chemical Engineering Journal*, *234*, 16–22. https://doi.org/https://doi.org/10.1016/j.cej.2013.08.060

Hutchins, R. A. (1973). New method simplifies design of activated carbon systems. *Chem. Eng.*, *80*, 133–138.

Jamwal, K. D., & Slathia, D. (2022). A review of defluoridation techniques of global and indian prominence. *Curr. World Environ*, *17*, 41–57.

Jawad, A. H., Azharul Islam, M., & Hameed, B. H. (2017). Cross-linked chitosan thin film coated onto glass plate as an effective adsorbent for adsorption of reactive orange 16. *International Journal of Biological Macromolecules*, *95*, 743–749. https://doi.org/https://doi.org/10.1016/j.ijbiomac.2016.11.087

Jin, X., Jiang, M., Du, J., & Chen, Z. (2014). Removal of Cr(VI) from aqueous solution by surfactant-modified kaolinite. *Journal of Industrial and Engineering Chemistry*, *20*(5), 3025–3032. https://doi.org/https://doi.org/10.1016/j.jiec.2013.11.038

Jo, J.-Y., Choi, J.-H., Tsang, Y. F., & Baek, K. (2021). Pelletized adsorbent of alum sludge and bentonite for removal of arsenic. *Environmental Pollution*, *277*, 116747. https://doi.org/https://doi.org/10.1016/j.envpol.2021.116747

Kanyora, A. K., Kinyanjui, T. K., Kariuki, S. M., & Chepkwony, C. K. (2014). Efficiency of various sodium solutions in regeneration of fluoride saturated bone char for de-fluoridation. *IOSR J Environ Sci. Toxicol. Food Technol*, *8*, 10–16.

Kebede, B., Beyene, A., Fufa, F., Megersa, M., & Behm, M. (2016). Experimental evaluation of sorptive removal of fluoride from drinking water using iron ore. *Applied Water Science*, *6*, 57–65.

Kumari, U., Mishra, A., Siddiqi, H., & Meikap, B. C. (2021). Effective defluoridation of industrial wastewater by using acid modified alumina in fixed-bed adsorption column: experimental and breakthrough curves analysis. *Journal of Cleaner Production*, *279*, 123645.

Lakiss, L., Gilson, J.-P., Valtchev, V., Mintova, S., Vicente, A., Vimont, A., Bedard, R., Abdo, S., & Bricker, J. (2020). Zeolites in a good shape: Catalyst forming by extrusion modifies their performances. *Microporous and Mesoporous Materials*, *299*, 110114. https://doi.org/https://doi.org/10.1016/j.micromeso.2020.110114

Laonapakul, T., Suthi, T., Otsuka, Y., Mutoh, Y., Chaikool, P., & Chindaprasirt, P. (2022). Fluoride adsorption enhancement of Calcined-Kaolin/Hydroxyapatite composite. *Arabian Journal of Chemistry*, *15*(11), 104220.

Lin, J., Wu, Y., Khayambashi, A., Wang, X., & Wei, Y. (2018). Preparation of a novel CeO2/SiO2 adsorbent and its adsorption behavior for fluoride ion. *Adsorption Science & Technology*, *36*(1–2), 743–761.

López-Cervantes, J., Sánchez-Machado, D. I., Sánchez-Duarte, R. G., & Correa-Murrieta, M. A. (2018). Study of a fixed-bed column in the adsorption of an azo dye from an aqueous medium using a chitosan–glutaraldehyde biosorbent. *Adsorption Science & Technology*, *36*(1–2), 215–232.

Lou, X.-Y., Boada, R., Simonelli, L., & Valiente, M. (2022). Enhanced arsenite removal by superparamagnetic iron oxide nanoparticles in-situ synthesized on a commercial cube-shape sponge: adsorption-oxidation mechanism. *Journal of Colloid and Interface Science*, *614*, 460–467. https://doi.org/https://doi.org/10.1016/j.jcis.2022.01.119

Maleki, F., Gholami, M., Torkaman, R., Torab-Mostaedi, M., & Asadollahzadeh, M. (2021). Cobalt(II) removal from aqueous solution by modified polymeric adsorbents prepared with induced-graft polymerization: Batch and continuous column study with analysis of breakthrough behaviors. *Environmental Technology & Innovation*, *24*, 102054. https://doi.org/https://doi.org/10.1016/j.eti.2021.102054

Mehta, D., Saharan, V. K., & George, S. (2023). Bio-adsorbent hydroxyapatite for drinking

water defluoridation: column performance modelling studies. *Environmental Science and Pollution Research*, 1–13.

Mittal, H., Alhassan, S. M., & Ray, S. S. (2018). Efficient organic dye removal from wastewater by magnetic carbonaceous adsorbent prepared from corn starch. *Journal of Environmental Chemical Engineering*, *6*(6), 7119–7131.

Mohammadi, A. A., Yousefi, M., Yaseri, M., Jalilzadeh, M., & Mahvi, A. H. (2017). Skeletal fluorosis in relation to drinking water in rural areas of West Azerbaijan, Iran. *Scientific Reports*, *7*(1), 17300.

Mohan, R., & Dutta, R. K. (2020). Continuous fixed-bed column assessment for defluoridation of water using HAp-coated-limestone. *Journal of Environmental Chemical Engineering*, *8*(4), 103840.

Mondal, P., & George, S. (2015). A review on adsorbents used for defluoridation of drinking water. *Reviews in Environmental Science and Bio/Technology*, *14*, 195–210.

Mondal, P., Mehta, D., Saharan, V. K., & George, S. (2018). Continuous column studies for water defluoridation using synthesized magnesium-incorporated hydroxyapatite pellets: experimental and modeling studies. *Environmental Processes*, *5*, 261–285.

Mourabet, M., El Rhilassi, A., El Boujaady, H., Bennani-Ziatni, M., & Taitai, A. (2017). Use of response surface methodology for optimization of fluoride adsorption in an aqueous solution by Brushite. *Arabian Journal of Chemistry*, *10*, S3292–S3302.

Mulugeta, E., Zewge, F., Annette Johnson, C., & Chandravanshi, B. S. (2014). A high-capacity aluminum hydroxide-based adsorbent for water defluoridation. *Desalination and Water Treatment*, *52*(28–30), 5422–5429.

Mustapha, S., Ndamitso, M. M., Abdulkareem, A. S., Tijani, J. O., Mohammed, A. K., & Shuaib, D. T. (2019). Potential of using kaolin as a natural adsorbent for the removal of pollutants from tannery wastewater. *Heliyon*, *5*(11), e02923. https://doi.org/https://doi.org/10.1016/j.heliyon.2019.e02923

Nur, T., Loganathan, P., Nguyen, T. C., Vigneswaran, S., Singh, G., & Kandasamy, J. (2014). Batch and column adsorption and desorption of fluoride using hydrous ferric oxide: Solution chemistry and modeling. *Chemical Engineering Journal*, *247*, 93–102.

Opoka, Tekola, & (ACEWM). (2023). *Aluminum hydroxide/hydroxyapatite composite for removal of fluoride from drinking water in a batch and continuous mode*.

Organization, W. H. (2004). *Guidelines for drinking-water quality* (Vol. 1). World Health Organization.

Osterwalder, L., Johnson, C. A., Yang, H., & Johnston, R. B. (2014). Multi-criteria

assessment of community-based fluoride-removal technologies for rural Ethiopia. *Science of the Total Environment*, *488*, 532–538.

Pandharipande, S. L., & Borkar, G. A. (2016). Synthesis, Characterization and Adsorption Study of Composite Adsorbent using Corncob and Cornstarch. *International Journal Of Science, Engineering And Technology Research*, *5*(5), 1484–1488.

Pang, C. Y., Issabayeva, G., Low, C. H., & Wong, M. C. (2021). Adsorption of fluoride from industrial wastewater using polymer adsorbents: a review. *IOP Conference Series: Earth and Environmental Science*, *945*(1), 12068.

Pathan, S., & Bose, S. (2018). Arsenic removal using "green" renewable feedstock-based hydrogels: current and future perspectives. *ACS Omega*, *3*(5), 5910–5917.

Pereira, A., Ferreira, A. F. P., Rodrigues, A., Ribeiro, A. M., & Regufe, M. J. (2022). Shaping of ZIF-8 and MIL-53(Al) adsorbents for CH4/N2 separation. *Microporous and Mesoporous Materials*, *331*, 111648. https://doi.org/https://doi.org/10.1016/j.micromeso.2021.111648

Poinern, G. E. J., Ghosh, M. K., Ng, Y.-J., Issa, T. B., Anand, S., & Singh, P. (2011). Defluoridation behavior of nanostructured hydroxyapatite synthesized through an ultrasonic and microwave combined technique. *Journal of Hazardous Materials*, *185*(1), 29–37.

Quintelas, C., Pereira, R., Kaplan, E., & Tavares, T. (2013). Removal of Ni (II) from aqueous solutions by an Arthrobacter viscosus biofilm supported on zeolite: from laboratory to pilot scale. *Bioresource Technology*, *142*, 368–374.

Raghav, S., Sapna, & Kumar, D. (2018). Cubical-shaped rods of pectin–hydroxyapatite composite for adsorption studies of fluoride by statistical method and adsorption experiments. *ACS Omega*, *3*(8), 9675–9688.

Razbe, N. R. N. (2013). Various options for removal of fluoride from drinking water. *IOSR Journal of Applied Physics*, *3*(2), 40–47.

Saikia, B. J., Parthasarathy, G., & Borah, R. R. (2022). Investigations of organic matter in meteorites using Fourier transform infrared and micro-Raman spectroscopic methods: Implications for origin of extraterrestrial organic matter. *Jour. Indian Geophys. Union*, *26*(1), 62–77.

Salifu, A. (2017). Laboratory-scale column filter studies for fluoride removal with aluminum (hydr) oxide coated pumice, regeneration and disposal. In *Fluoride Removal from Groundwater by Adsorption Technology* (pp. 116–160). CRC Press.

Sheng, L., Zhang, Y., Tang, F., & Liu, S. (2018). Mesoporous/microporous silica materials:

preparation from natural sands and highly efficient fixed-bed adsorption of methylene blue in wastewater. *Microporous and Mesoporous Materials*, *257*, 9–18.

Siaurusevičiūtė, I., & Albrektienė, R. (2021). Removal of fluorides from aqueous solutions using exhausted coffee grounds and iron sludge. *Water*, *13*(11), 1512.

Singh, J., Singh, P., & Singh, A. (2016). Fluoride ions vs removal technologies: a study. *Arabian Journal of Chemistry*, *9*(6), 815–824.

Sosnik, A., & Seremeta, K. P. (2015). Advantages and challenges of the spray-drying technology for the production of pure drug particles and drug-loaded polymeric carriers. *Advances in Colloid and Interface Science*, *223*, 40–54.

Sugashini, S., & Sheriffa Begum, K. M. (2013). Column adsorption studies for the removal of Cr (VI) ions by ethylamine modified chitosan carbonized rice husk composite beads with modelling and optimization. *Journal of Chemistry*, *2013*.

Talat, M., Mohan, S., Dixit, V., Singh, D. K., Hasan, S. H., & Srivastava, O. N. (2018). Effective removal of fluoride from water by coconut husk activated carbon in fixed bed column: Experimental and breakthrough curves analysis. *Groundwater for Sustainable Development*, *7*, 48–55.

Teutli-Sequeira, A., Solache-Ríos, M., Martínez-Miranda, V., & Linares-Hernández, I. (2015). Behavior of fluoride removal by aluminum modified zeolitic tuff and hematite in column systems and the thermodynamic parameters of the process. *Water, Air, & Soil Pollution*, *226*, 1–15.

Thomas, H. C. (1944). Heterogeneous Ion Exchange in a Flowing System. *Journal of the American Chemical Society*, *66*(10), 1664–1666. https://doi.org/10.1021/ja01238a017

Tomar, V., & Kumar, D. (2013). A critical study on efficiency of different materials for fluoride removal from aqueous media. *Chemistry Central Journal*, *7*, 1–15.

Uddin, M. K. (2017). A review on the adsorption of heavy metals by clay minerals, with special focus on the past decade. *Chemical Engineering Journal*, *308*, 438–462.

Valizadeh, B., Nguyen, T. N., & Stylianou, K. C. (2018). Shape engineering of metal–organic frameworks. *Polyhedron*, *145*, 1–15.

Vertruyen, B., Eshraghi, N., Piffet, C., Bodart, J., Mahmoud, A., & Boschini, F. (2018). Spray-drying of electrode materials for lithium-and sodium-ion batteries. *Materials*, *11*(7), 1076.

Vivek Vardhan, C. M., & Srimurali, M. (2016). Removal of fluoride from water using a novel sorbent lanthanum-impregnated bauxite. *SpringerPlus*, *5*, 1–18.

Wan, K., Huang, L., Yan, J., Ma, B., Huang, X., Luo, Z., Zhang, H., & Xiao, T. (2021).

Removal of fluoride from industrial wastewater by using different adsorbents: A review. *Science of the Total Environment*, *773*, 145535.

Wang, S., Li, C., Copeland, L., Niu, Q., & Wang, S. (2015). Starch retrogradation: A comprehensive review. *Comprehensive Reviews in Food Science and Food Safety*, *14*(5), 568–585.

Wang, Z., Zhai, Y., Wang, T., Wang, B., Peng, C., & Li, C. (2020). Pelletizing of hydrochar biofuels with organic binders. *Fuel*, *280*, 118659. https://doi.org/https://doi.org/10.1016/j.fuel.2020.118659

Wimalawansa, S. J. (2013). Purification of contaminated water with reverse osmosis: effective solution of providing clean water for human needs in developing countries. *International Journal of Emerging Technology and Advanced Engineering*, *3*(12), 75–89.

Xiao, G., Zhang, X., Su, H., & Tan, T. (2013). Plate column biosorption of Cu(II) on membrane-type biosorbent (MBS) of Penicillium biomass: Optimization using statistical design methods. *Bioresource Technology*, *143*, 490–498. https://doi.org/https://doi.org/10.1016/j.biortech.2013.06.035

Yadav, K. K., Gupta, N., Kumar, V., Khan, S. A., & Kumar, A. (2018). A review of emerging adsorbents and current demand for defluoridation of water: Bright future in water sustainability. *Environment International*, *111*, 80–108.

Yagub, M. T., Sen, T. K., Afroze, S., & Ang, H. M. (2015). Fixed-bed dynamic column adsorption study of methylene blue (MB) onto pine cone. *Desalination and Water Treatment*, *55*(4), 1026–1039.

Yeskendir, B., Dacquin, J.-P., Lorgouilloux, Y., Courtois, C., Royer, S., & Dhainaut, J. (2021). From metal–organic framework powders to shaped solids: recent developments and challenges. *Materials Advances*, *2*(22), 7139–7186.

YOON, Y. H. E. E., & NELSON, J. H. (1984). Application of Gas Adsorption Kinetics — II. A Theoretical Model for Respirator Cartridge Service Life and Its Practical Applications. *American Industrial Hygiene Association Journal*, *45*(8), 517–524. https://doi.org/10.1080/15298668491400205

Zewge, F. (2016). Combined aluminium sulfate/hydroxide process for fluoride removal from drinking water. *Bulletin of the Chemical Society of Ethiopia*, *30*(3), 391–401.

Zhang, G., Qu, J., Liu, H., Cooper, A. T., & Wu, R. (2007). CuFe2O4/activated carbon composite: A novel magnetic adsorbent for the removal of acid orange II and catalytic regeneration. *Chemosphere*, *68*(6), 1058–1066.

https://doi.org/https://doi.org/10.1016/j.chemosphere.2007.01.081

Zhang, Y.-X., & Jia, Y. (2016). Fluoride adsorption onto amorphous aluminum hydroxide: Roles of the surface acetate anions. *Journal of Colloid and Interface Science*, *483*, 295–306. https://doi.org/https://doi.org/10.1016/j.jcis.2016.08.054

Zhang, Y., Xiong, L., Xiu, Y., & Huang, K. (2019). Defluoridation in fixed bed column filled with Zr (IV)-loaded garlic peel. *Microchemical Journal*, *145*, 476–485.

Zhao, B., Zhang, Y., Dou, X., Wu, X., & Yang, M. (2012). Granulation of Fe–Al–Ce trimetal hydroxide as a fluoride adsorbent using the extrusion method. *Chemical Engineering Journal*, *185–186*, 211–218. https://doi.org/https://doi.org/10.1016/j.cej.2012.01.085

Zhao, H., Zhou, F., Ma, C., Wei, Z., & Long, W. (2022). Bonding mechanism and process characteristics of special polymers applied in pelletizing binders. *Coatings*, *12*(11), 1618.

Appendix

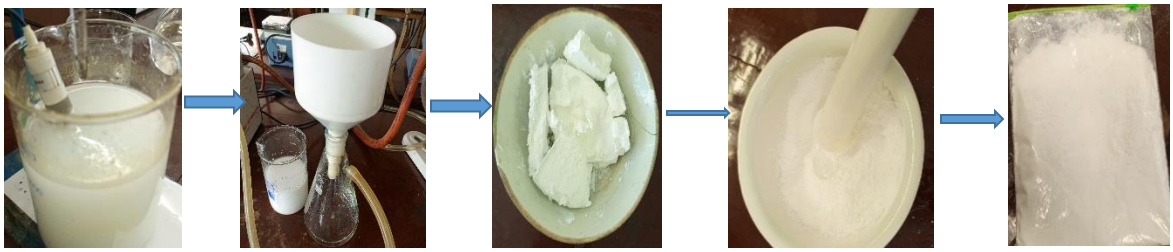

Figure 11: Synthesis of Aluminium Hydroxide through precipitation method

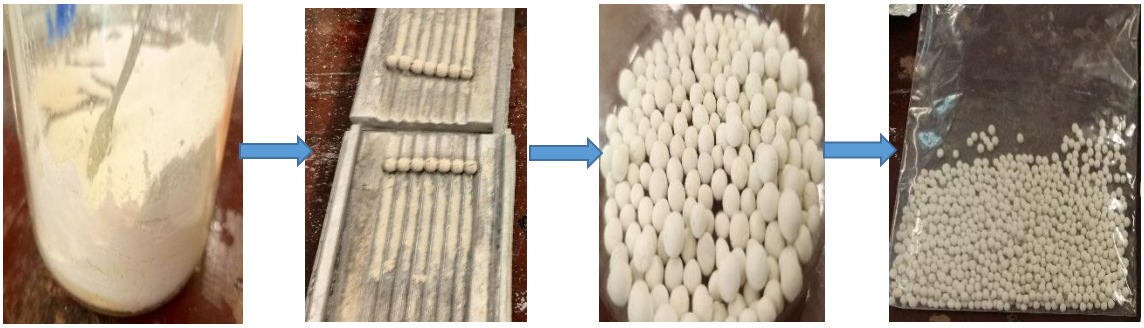

Figure 12: procedure used in shaping of $Al(OH)_3$/HAP adsorbent composite into spherical shapes

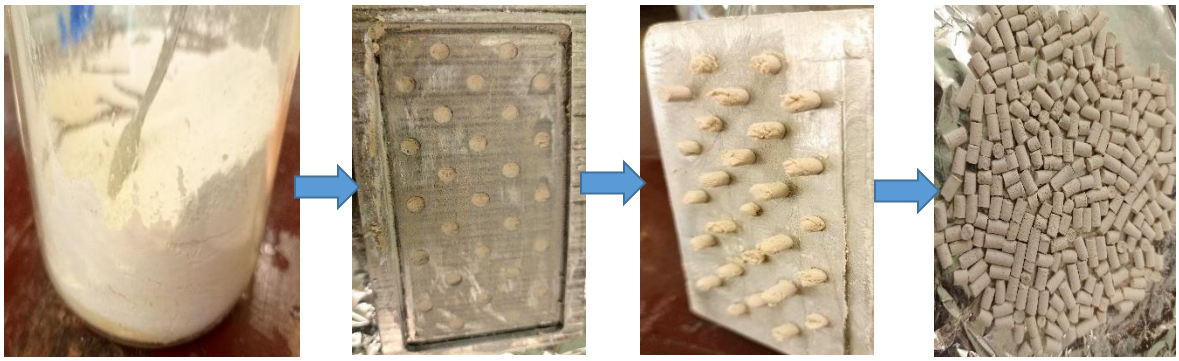

Figure 13: Procedure used in shaping of $Al(OH)_3$/HAP adsorbent composite into cylindrical shapes

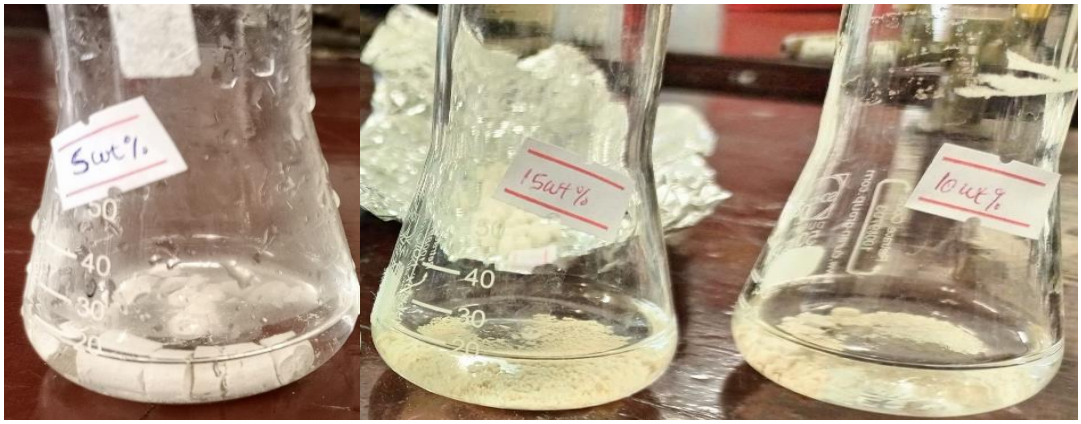

Figure 14: Testing the bentonite pellet's stability in aqueous solution with 10 mg/l fluoride concentration (a) 5 wt. %, (b) 15 wt. %, (c) 10 wt. %

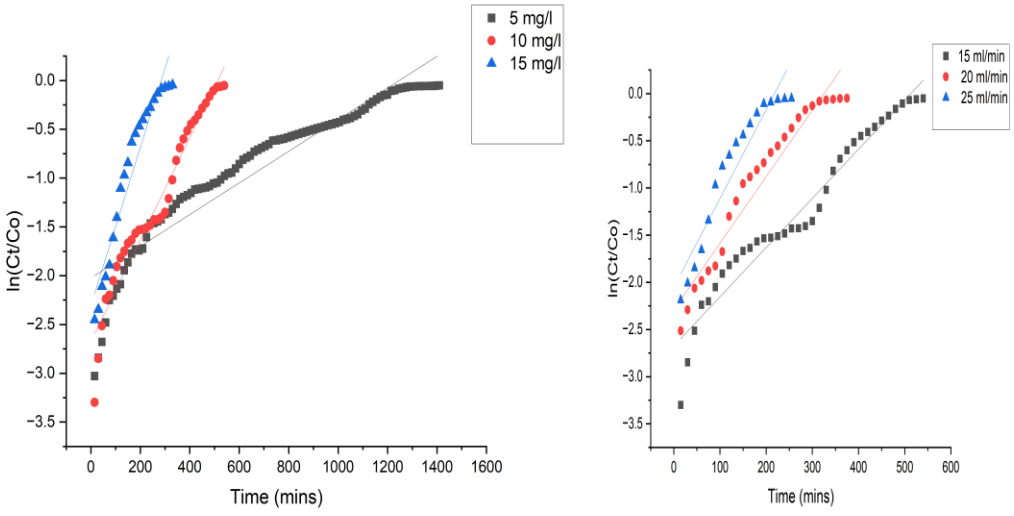

(a) (b)

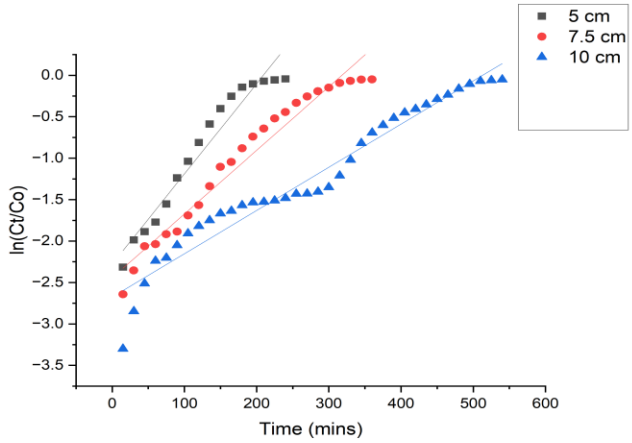

(c)

Figure 15: Adams-Bohart model linear fitting breakthrough curve for varying (a)initial fluoride concentration, (b) flow rates, and (c)bed heights

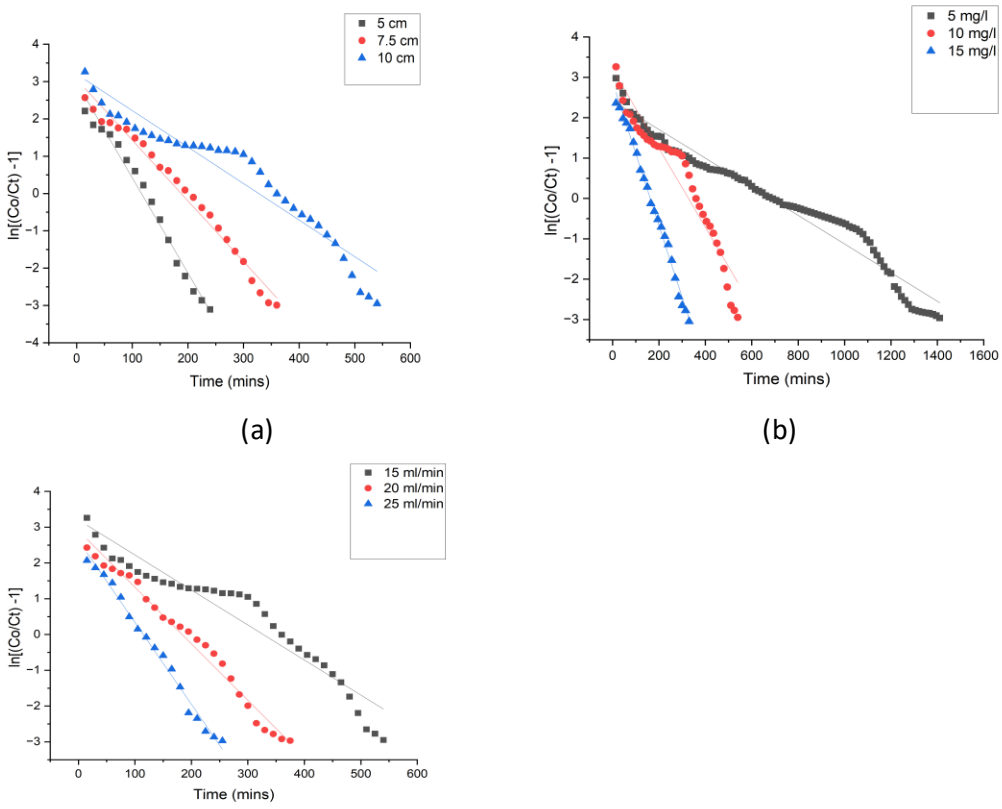

Figure 16: Thomas model linear fitting to breakthrough curves of various adsorption parameters, (a)bed height, (b) initial fluoride concentration, and (c) flow rate

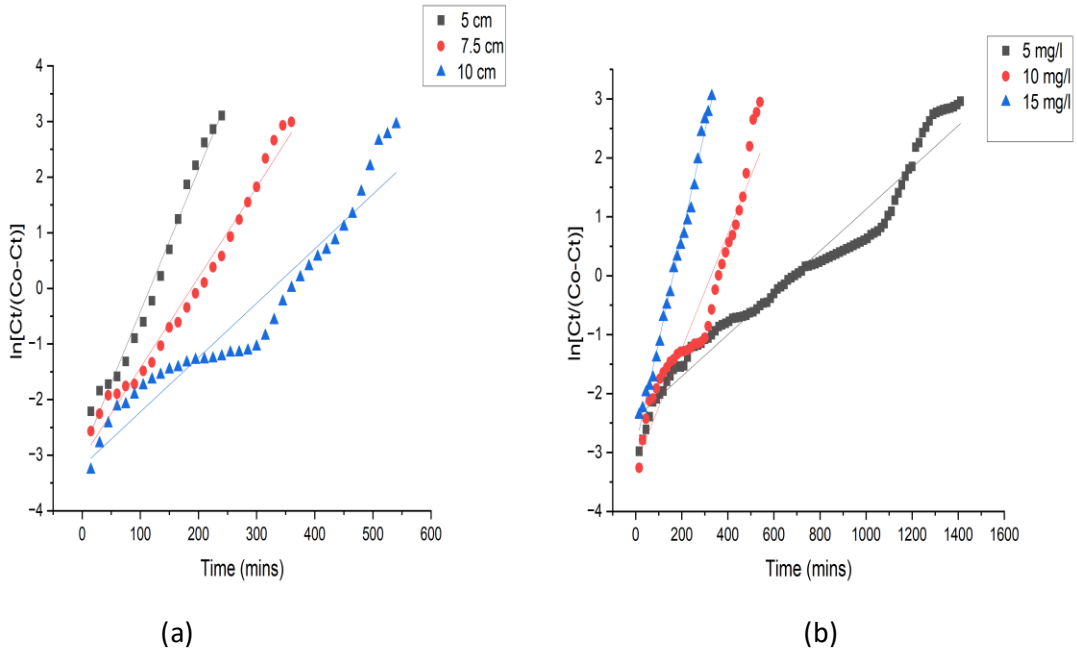

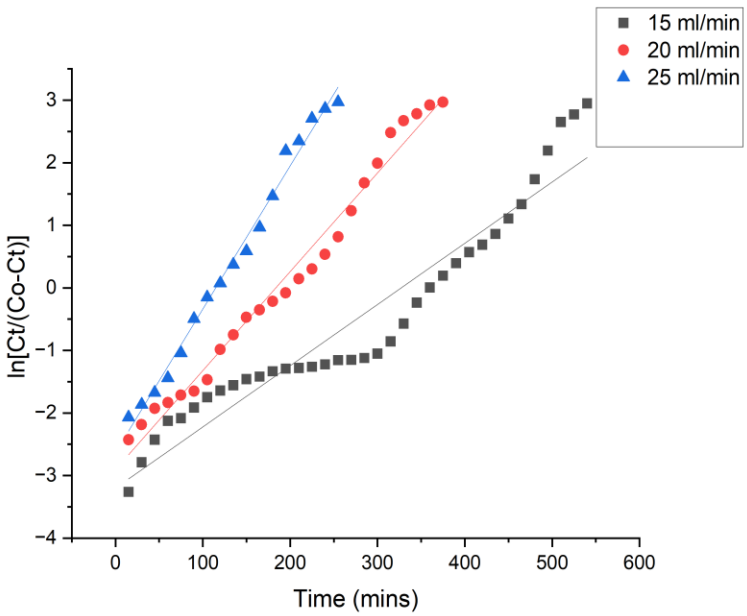

(c)

Figure 17:Yoon-Nelson linear fitting to breakthrough of varying,(a) bed height, (b) initial fluoride concentration, (c) flow rate

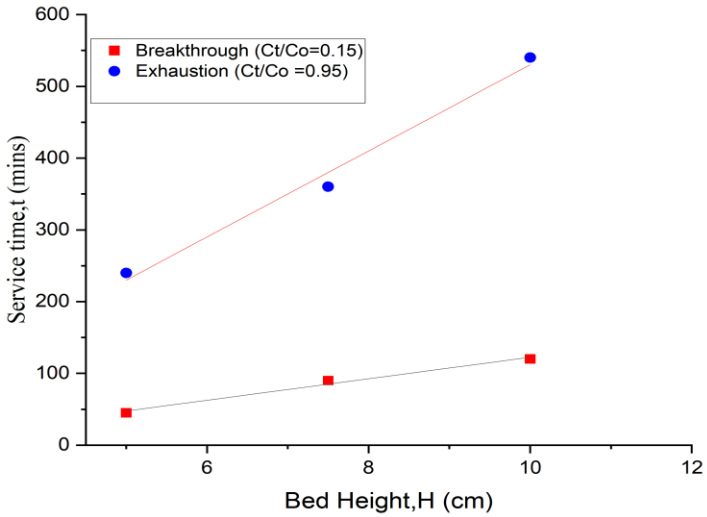

Figure 18:BDST model plots for Al(OH)3/Hap pellets breakthrough and exhaustion point